Master's thesis
Astronomy

Spin and shape analyses for the slowly rotating asteroid (39420) 2084 T-2

Grigori Fedorets

2013

Tutor: Dr. Mikael Granvik

Censors: Prof. Karri Muinonen
Dr. Mikael Granvik

UNIVERSITY OF HELSINKI
Department of Physics

PL 64 (Gustaf Hällströmin katu 2)
00014 Helsingin yliopisto

HELSINGIN YLIOPISTO — HELSINGFORS UNIVERSITET — UNIVERSITY OF HELSINKI

Tiedekunta — Fakultet — Faculty	Laitos — Institution — Department
Matemaattis-luonnontieteellinen tiedekunta	Fysiikan laitos

Tekijä — Författare — Author
Grigori Fedorets

Työn nimi — Arbetets titel — Title

Hitaasti kierivän asteroidin (39420) 2084 T-2 pyörimis- ja muotoanalyysi

Oppiaine — Läroämne — Subject
Tähtitiede

Työn laji — Arbetets art — Level	Aika — Datum — Month and year	Sivumäärä — Sidoantal — Number of pages
Pro gradu	2013	89 sivua

Tiivistelmä — Referat — Abstract

Asteroidien pyörimistä tutkitaan jotta saataisiin tietoa asteroidien fysikaalista ominaisuuksista ja prosesseista. Pyörimisperiodijakauma eri asteroidikokoluokissa kuvaa ei-gravitaatiovoimien merkitystä riippuen asteroidin koosta. Tiettyjen pyörimistilojen puuttuminen pyörimisjakaumasta asettaa rajoituksia erikokoisten asteroidien sisäiselle rakenteelle.

Suurin osa fotometrisistä valokäyristä saaduista asteroidien pyörimisperiodeista on ratkaistu nopeasti pyöriville kappaleille. Hitaasti pyörivän asteroidin pyörimisperiodin ratkaiseminen vaatii huomattavasti enemmän havaintoaikaa kuin nopeasti pyörivän kappaleen. Näin ollen valokäyräseurantaohjelmissa, joissa havaintoaikaa jaetaan tasaisesti asteroidien kesken, vain nopeasti pyöriville asteroideille on mahdollista ratkaista tarkkoja pyörimisperiodeja.

Tutkielma keskittyy asteroidien pyörimisen eri näkökohtiin. Tutkielmassa kuvaillaan erilaisia metodeja, joiden avulla voidaan määrittää asteroidien pyörimisperiodeja ja muotomalleja. Lisäksi tutkielmassa käsitellään fysikaalisia mekanismeja, jotka vaikuttavat asteroidien pyörimiseen. Painopiste on päävyöhykeasteroideissa ja hitaasti pyörivissä kappaleissa.

Canada-France-Hawaii -kaukoputkella toteutettu TALCS-seurantaohjelma (Masiero et al. 2009) oli yksi ensimmäisistä systemaattisista asteroidien valokäyräseurantaohjelmista. Yksi valituista asteroideista on Hungaria-populaation asteroidi (39420) 2084 T-2. Masiero et al. (2009) antaa pyörimisperiodin tulokseksi 105 $\pm$ 21 tuntia, mikä on suhteellisen epätarkka tulos verrattuna saatuihin nopeasti pyörivien asteroidien periodien virherajoihin. Tässä työssä esitellään päivitetty periodi-tulos sekä ehdotus asteroidin konveksiksi muotomalliksi (Kaasalainen & Torppa 2001, Kaasalainen et al. 2001). Lisäksi arvoidaan, onko kyseinen kohde mahdollisesti kaksoisasteroidi ja pyöriikö se pääakselinsa ympäri.

Avainsanat — Nyckelord — Keywords
asteroidi, pyöriminen, fotometria, MBA, periodi

Säilytyspaikka — Förvaringsställe — Where deposited

Muita tietoja — övriga uppgifter — Additional information

HELSINGIN YLIOPISTO — HELSINGFORS UNIVERSITET — UNIVERSITY OF HELSINKI

Tiedekunta — Fakultet — Faculty	Laitos — Institution — Department
Faculty of Mathematics and Natural Sciences	Department of Physics

Tekijä — Författare — Author
Grigori Fedorets

Työn nimi — Arbetets titel — Title

Spin and shape analyses for the slowly rotating asteroid (39420) 2084 T-2

Oppiaine — Läroämne — Subject
Astronomy

Työn laji — Arbetets art — Level	Aika — Datum — Month and year	Sivumäärä — Sidoantal — Number of pages
Master's thesis	2013	89 pages

Tiivistelmä — Referat — Abstract

The investigation of rotation of asteroids is an important means to deriving information about their physical properties and processes using ground-based instrumentation. The rotation rate distribution imply the significance of non-gravitational forces depending on the size of the asteroid. The absence of certain rotation rates in the asteroid population poses constraints on the inner structure of asteroids of different sizes.

The majority of rotation periods of asteroids solved from photometric lightcurves belong to fast rotators. The observation time required for obtaining an accurate period estimate is substantially longer for a slowly rotating asteroid than for a rapidly rotating asteroid. Therefore, lightcurve surveys with limited observation time which allocate the same amount of time for all asteroids, are expected to only produce accurate periods for asteroids with short rotation periods.

This thesis concentrates on various aspects of asteroid rotation. Methods used to obtain asteroid rotation periods and shape models are discussed. Also, physical mechanisms affecting the rotation of asteroids are considered. The focus is on the main-belt objects and slowly rotating bodies.

The Thousand Asteroid Lightcurve Survey (Masiero et al. 2009) carried out with the Canada-France-Hawaii Telescope was one of the first systematic asteroid lightcurve surveys. One of the objects selected for follow-up was Hungaria asteroid (39420) 2084 T-2. Masiero et al. (2009) quoted a rotation period of 105 ± 21 h which is a relatively inaccurate solution, especially compared to the solutions for the fast rotators. In this work we present an updated period fit as well as a possible convex shape solution (Kaasalainen & Torppa 2001, Kaasalainen et al. 2001) for the asteroid. The possibility that the investigated asteroid is a close binary or a non-principal-axis rotator is also discussed.

Avainsanat — Nyckelord — Keywords
asteroid, rotation, photometry, MBA, period

Säilytyspaikka — Förvaringsställe — Where deposited

Muita tietoja — övriga uppgifter — Additional information

Contents

List of abbreviations

NEA Near-Earth asteroid

MBA Main-belt asteroid

TALCS Thousand Asteroid Lightcurve Survey

YORP Yarkovsky-O'Keefe-Radzievskii-Paddock effect

Pan-STARRS Panoramic Survey Telescope And Rapid Response System

JWST James Webb Space Telescope

E-ELT European Extremely Large Telescope

MPC Minor Planet Circular

SAM Short-axis mode

MJD Modified Julian Date

KOALA Knitted Occultation, Adaptive-optics and Lightcurves Approach

DAMIT Database of Asteroid Models from Inversion Techniques

rms root mean square

LAM Long-axis mode

1. Introduction

1.1 Overview of asteroids

Asteroids (Greek: astereides, 'star-like') are small Solar System bodies comprising a significant bulk of the minor bodies orbiting the Sun. There is no explicit definition for an asteroid and previously all non-cometary minor bodies of the Solar System were classified as asteroids. However, the increased knowledge about the distant minor bodies of the Solar System (transneptunian objects, centaurs) suggests that their surface resembles comets rather than asteroids. Therefore, in literature the term 'asteroid' can refer either to all minor bodies on a circumsolar orbit without any notable cometary activity or those of them with the outer boundary being the orbit of Jupiter. Colloquially, also the term 'small Solar System body' is used.

Another problem with defining asteroids is that the size distribution of bodies in the Solar System is somewhat continuous. It ranges from interplanetary dust particles to planets, so boundaries between object classes are conventional rather than based on physical differences. The increasing rate of discovery of large transneptunian objects forced the astronomical community to define specific boundaries for different types of Solar System bodies (IAU 2006). The previously largest asteroid Ceres and smallest planet Pluto were categorized into a new class of dwarf planets along with several newly discovered transneptunian bodies. According to the new definition, the upper boundary of a small Solar System body and a lower boundary

of a dwarf planet is the body's inability to obtain a hydrostatic equilibrium state (i.e. a nearly spherical shape). A distinction between a dwarf planet and a planet is the ability of the latter to clear its orbit and nearby neighbourhood from other bodies.

On the other side of the size distribution is the problem of defining a boundary between asteroids and meteoroids and interplanetary dust particles. In order to be observable and mutually distinguishable (a *de-facto* requirement) asteroids are required to be macroscopic bodies.

Asteroids are spread throughout the entire Solar System. The major dynamically stable populations of asteroids are situated between the orbits of Mars and Jupiter, (main-belt asteroids, MBAs), near Jupiter's Lagrange points L_4 and L_5 (Jupiter Trojans) and beyond the orbit of Neptune (transneptunian objects, TNOs, which include the classical Kuiper belt objects and scattered disk objects).

While the asteroids in the stable populations can retain their orbits for periods comparable with the life time expectancy of the Sun, the established areas are infiltrated with narrow unstable mean-motion and secular resonance gaps. Asteroids that are driven to these resonance areas are likely to have their orbits altered significantly. An asteroid's orbit can drift into a resonance as a result of mutual collisions or thermal effects. Furthermore, the boundaries of resonance areas are subject to change due to constantly osculating orbital elements of planets in the Solar System.

The dynamically unstable asteroid populations include the Centaurs, i.e., bodies in a transitional phase from the Kuiper belt to the inner part of the Solar System (Horner et al. 2004) with the semimajor axes between those of Jupiter and Neptune; the Near-Earth asteroids (NEAs) whose orbits come close to and sometimes intersect Earth's orbit, and Mars crossers – asteroids in a transitional phase from the main belt to the innermost parts of the Solar System. A body on an unstable orbit is destined either to become disintegrated in a collision with the Sun or any other

body of the Solar System, or to be ejected onto an interstellar orbit after a close encounter with Jupiter.

The constantly changing nature of NEA orbits calls to their constant monitoring. The potential threat to the Earth's biosphere by a possible collision with such an object maintains a constant level of interest in all aspects of asteroid sciences, although, the NEA population is the main target of interest with regards to the potential hazard.

The risk posed to the Earth by a collision with a passing body was generally acknowledged after the Alvarez hypothesis of the Cretatious-Paleogene extinction event, which suggested that the mass extinction 65 million years ago was caused by a colliding asteroid or comet (Alvarez et al. 1980). The remnant of this event is the Chicxulub crater on the Yucatan peninsula in Mexico as well as the worldwide iridium-rich layer in the geological Cretatious-Paleogene (Tertiary) boundary. Another important event in raising the awareness on the possibilities of the outcome in the case of an impact hazard was the collision of disintegrated parts of comet Shoemaker-Levy 9 with Jupiter in July 1994 (Noll et al. 1996).

The main asteroid belt is the continuous source for the NEA population (Michel et al. 2005). The mechanisms affecting asteroids in the main belt are vital to understanding the origin and prediction of dynamics of the NEA population.

The first asteroid, (1) Ceres (now classified as a dwarf planet (IAU 2006)), was discovered on an orbit located between the orbits of Mars and Jupiter in 1801, soon followed by the discoveries of three other large asteroids (Foderà Serio et al. 2002). The discovery of these first asteroids opened the way for modern orbit determination, pioneered by Gauss. After these discoveries, however, the revelation of new asteroids stalled until the middle of the nineteenth century. In the second half of the nineteenth century several asteroids were found each year. It was not until 1890 and Max Wolf's groundbreaking contribution when photography became useful in

search for asteroids (Karttunen 2009). Since then, the discovery rate of new asteroids has being constantly increasing. Last decades have seen the introduction of modern techniques, such as CCD cameras and automatic asteroid surveys, including the ongoing Catalina Sky Survey or Pan-STARRS (Panoramic Survey Telescope And Rapid Response System), which is currently entering its full-operation mode. The introduction of these new methods and instruments have increased the discovery rates even higher. As a result, currently over 500 000 asteroids have been discovered. All known minor bodies within the orbit of Jupiter are presented in Fig. 1.1.

The main asteroid belt is a significant source for obtaining data about the asteroids. It is well observable both astrometrically and photometrically and provides a consistent, dynamically evolved population. Besides being a source for NEAs, the main asteroid belt displays a lot of other scientific interest. The endogenic geological processes of asteroids, such as melting and crystallisation, were finalized already during the birth of the Solar System. The only major geological processes currently present in asteroids are purely exogenic, e.g. collisions and space weathering. Therefore, main-belt asteroids are a unique natural laboratory for exploring the early Solar System evolution. Various significant events in the history of the Solar System may be imprinted into the dynamical and physical properties of the main asteroid belt population.

Among the stellar bodies, asteroids have the privilege of being explored by virtually any method available in astronomy. In addition to the traditional astrometry, photometry and spectrometry, also radar observations and even sample mineralogic analysis from *in situ* missions are carried out occasionally.

Asteroids were initially formed in the accretion process during the formation of the Solar System. Asteroids' shapes are a result of catastrophic collisional evolution between the initial population and their fragments and, consequently, their

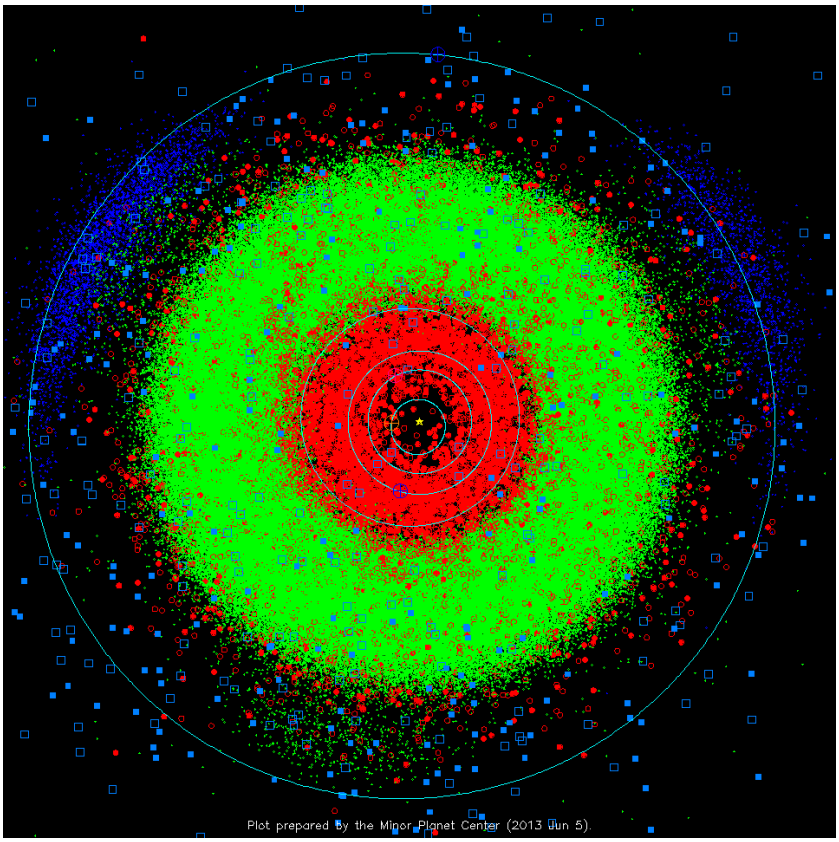

Figure 1.1: The plot of all known Solar System objects situated in the inner Solar System as of June 5th 2013 projected on the ecliptic plane. The orbits of planets are drawn in turquose. The small red, green, and blue points represent NEAs, well known MBAs and Jupiter Trojans, respectively. The open red circles are objects observed only during a single apparition. Open and filled blue squares are non-periodic and periodic comets, respectively. The plot has been prepared by Gareth Williams/Minor Planet Center.

dissipation and reaccumulation into loosely tied bodies known as “rubble piles”. These processes have shaped the main-belt asteroids throughout the entire course of existence of the Solar System.

1.2 Overview of asteroid rotation

The essential term in field of investigation of asteroid rotation is the lightcurve. A lightcurve is defined as a sequence of brightness measurements as a function of time or rotational phase. Typically, a single lightcurve consists of one night's observations but especially in the case of a slow rotator, it is often convenient to combine observations of several nights into a single lightcurve.

The rotation of asteroids is mainly observed through photometric curves during several nights. A particular asteroid is not continuously detectable from the Earth. A time arc during which an asteroid is detectable from the Earth is called an apparition, and it occurs when the asteroid and the Earth are on the same side from the Sun. In addition, the length of uninterrupted asteroid lightcurves is limited by the night time, since there are no major observatories located in the arctic or antarctic regions and observation time of spaceborne observatories is very limited.

In order to get more data, photometric lightcurves can be supplemented by infrared observations, which can be used to deduct the size and albedo of the asteroid. Other techniques implemented in asteroid observations are disk-resolved imaging, occultation observations and particularly, radar observations, from which high precision rotation period information can be obtained. Naturally, in order to obtain the most reliable information, all data from different observations must be combined.

The span of observed rotation periods of asteroids varies from 36 seconds to 42 days (Masiero et al. 2009). There are two independent widely used methods to obtain the rotational period of an asteroid from photometric data: the Fourier series method (Harris et al. 1989) and the inverse method aiming for the solution of

period, shape, and pole of asteroids simultaneously by fitting a convex model in the lightcurve (Kaasalainen & Torppa 2001, Kaasalainen et al. 2001). Both methods work best for asteroids with short rotation periods with substantial observational coverage, but the latter method is possible to adjust for determining also longer periods.

The rotation rate distribution of asteroids is used to investigate the forces and processes affecting the asteroid belt and, more widely, the Solar System. The rotation rate distribution of asteroids of different sizes is important in various aspects of asteroid studies. The rotation rate distribution applied to different size populations imply the significance of non-gravitational forces depending on the size of the asteroid. The absence of certain rotation rates in the asteroid population poses constraints on the inner structure of asteroids of different sizes – the presence of very fast rotators only among the smallest of asteroids is strong evidence for the hypothesis that the substantial fraction of small and mid-sized asteroids are "rubble piles".

The rotation rate of asteroids is a limiting factor for asteroid shapes – since the inner structure of many asteroids is likely to be very weak, very fast rotation would not be possible for such bodies, as it would result in their disintegration. Some recent results (Cotto-Figueroa et al. 2013) indicate that the shapes of rubble piles are not rigid but rather constantly changing into a lower energy state, having been continuously subject to the YORP torque.

Some asteroids have well established physical properties due to extensive observations while some may have been observed only once. In order to classify the reliability of fitted lightcurves, a lightcurve quality parameter (U) has been implemented (Harris & Young 1983). It is a scale from 0 to 3, where a higher number corresponds to the higher accuracy of solution. The determined values of periods should be always reported with the quality parameter and the assessment of relia-

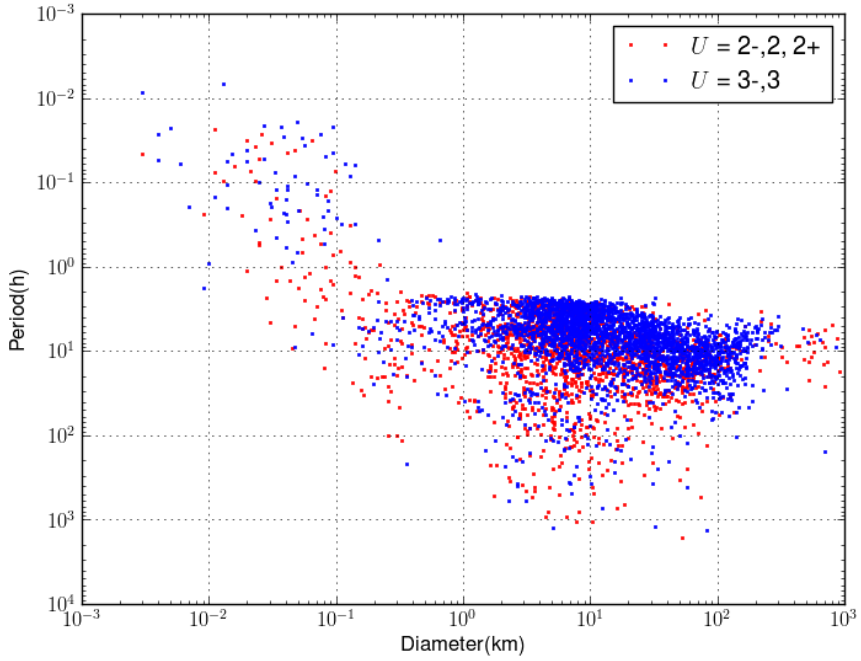

Figure 1.2: All known asteroids with a period and diameter having a reliability parameter $U \geq 2-$ listed in the lightcurve database (Warner et al. 2009a).

bility of periods should be always performed. The periods with a quality parameter less than 2- are considered unreliable.

The distribution of reliable periods of asteroids as a function of their diameter is presented in Fig. 1.2.

The shapes of asteroids are irregular which permits solving the rotational period from a lightcurve because repeatable features are prominent. The inability to solve the shape model of an asteroid may be caused by the fact that the asteroids might not necessarily be rotating around their principal axes. The principal-axis rotation is, however, the lowest energy state for asteroid rotations and is therefore usual.

As collisions have the most notable effect on all asteroid properties, it is natural to start building the picture of asteroid rotation distributions through gaining insight into what kind of outcome the collisions bring along. The Maxwellian rota-

tion rate distribution is an expected outcome for a solely-collisional evolved system. The definition of the Maxwellian distribution requires that all three axial rotational components are distributed among the normal distribution with zero mean values and same variation at both ends. The evolution of a collisionally evolved system permits such an outcome (Salo 1987). The existing deviations from the Maxwell distribution indicate that other processes than collisions have been involved in forming the existing asteroid rotation rate distribution.

The distinction of asteroids into subgroups according to their size is more or less conventional. This thesis uses the convention presented in Pravec et al. (2002), where large asteroids are those with a diameter over 40 km, small asteroids have a diameter between 0.15 km and 10 km whereas smallest asteroids have a diameter smaller than 0.15 km. This leaves the mid-sized asteroids to have the diameters between 10 km and 40 km. This convention is widely used in the literature concerning asteroid rotations due to different properties of rotation rate distributions for each group.

The previously mentioned division of the asteroids into different size groups is justified by the fact that the rotation rate of the asteroids varies considerably with size. The rotation rate distribution of different size groups is presented in Fig. 1.3. In the rotation rate distribution, four categories of asteroids are distinguished (Pravec et al. 2002). The rotation-number distribution of large asteroids (d $>$ 40 km) follows the Maxwell distribution closely. Some of the largest main-belt asteroids may have not been completely disintegrated during the entire existence of the Solar System.

The distribution of small and mid-sized asteroids is of particular interest. While the main trend of these asteroids is established to be the Maxwellian distribution, there is also a significant increase of number of slow rotators which requires an explanation (Pravec et al. 2002). Furthermore, the rotation properties of asteroids can be a key to distinguish binary and contact-binary asteroids from ordinary

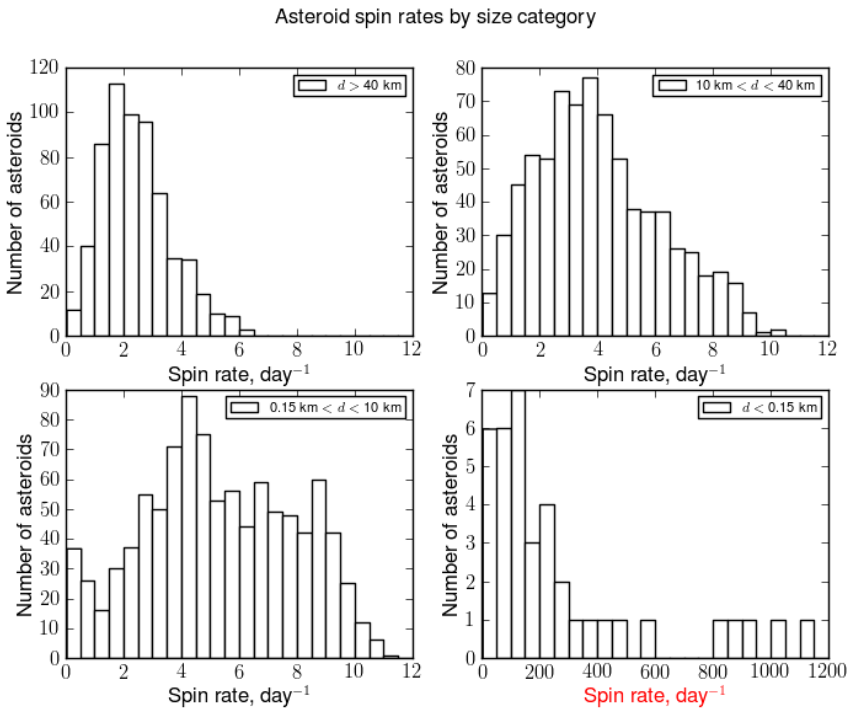

Figure 1.3: The rotation rate distribution of asteroids with $U \geq 2-$ by size category. Large asteroids follow the Maxwell distribution, small and medium-sized ones have excesses in fast and slow rotators. Smallest asteroids are plotted on an entirely different scale due to their completely different, generally very fast rotation. Data is from the Asteroid Lightcurve Database (Warner et al. 2009a).

ones because close binary asteroid systems are often observed as a single slowly rotating body. The search for binaries is therefore performed among slowly rotating small and middle-sized asteroids. In some cases, however, the resolution of ground-based observatories supplied with adaptive optics is sufficient to separately observe the bodies in a binary (Merline et al. 1999) or even ternary (Marchis et al. 2005) system.

The distributions of small (0.15 km $< d <$ 10 km) asteroids introduces a barrier of ca. 12 rotations/day beyond which there are only uncertain period solutions. This implies that almost all small asteroids are "rubble piles" and shattered objects because higher rotation rates lead to fragmentation of an asteroid into small bod-

ies. Furthermore, there is an excess of both small and fast rotators compared to the Maxwellian distribution, as is among the medium-sized (10 km $< d <$ 40 km) asteroids.

The smallest objects ($d <$ 0.15 km) consist mostly of very fast rotators. In fact, the majority of very small asteroids has a rotation period less than 2 hours. The upper size boundary of 0.15 km suggests that monolithic bodies higher than that size are unable to survive in the collision-driven population for a long time. The mean rotation rates of asteroids do not depend on their taxonomic class. The lack of fast large rotators supported the widely accepted theory that most asteroids, apart from the smallest ones, are "rubble piles". However, recent work by Scheeres & Sanchez (2012) based on surface properties of asteroid (25143) Itokawa implies that mutual van der Waals forces between particles comprising the smallest "rubble piles" are strong enough to allow short rotation periods.

The largest constraints in the rotational data of asteroids have been the uncertainty of long periods, low amplitudes and faint magnitudes. In order to acquire more precise rotational data, at least two major asteroid lightcurve surveys have been conducted in the last ten years: the Thousand Asteroid Lightcurve Survey also known as TALCS (Masiero et al. 2009), and the Photometric Survey for Asynchronous Binary Asteroids or BinAstPhotSurvey (Pravec et al. 2008).

In addition to regularly rotating objects, some asteroids also experience non-principal-axis rotation. These bodies are also known as tumbling asteroids. For some very slow irregularly-shaped rotating asteroids (Harris 1994) the non-principal-axis rotation state is most preferential in terms of lowest rotation energy state.

1.3 Hungaria asteroids

The Hungaria asteroids are a distinct isolated asteroid population located at the inner edge of the main asteroid belt. They are named by the largest body among

them, i.e., (434) Hungaria. The rough boundary values of the Hungaria region are 1.78 AU and 2.0 AU for semimajor axis, 16° and 34° for inclination while 0.18 is an upper boundary for eccentricity (Warner et al. 2009b). Currently, there are about 5000 known Hungaria objects. The location of Hungaria asteroids in the semimajor axis - eccentricity - inclination space is presented in Figs 1.4 and 1.5.

Due to high inclination and, particularly, low eccentricity, Hungaria asteroids avoid been disturbed by Mars when the latter is on a low-eccentricity orbit. On the other hand, the Hungaria asteroids do not intersect with major resonance areas. The outer boundaries of the Hungaria region are shaped by various secular resonances with Jupiter and Saturn (Milani et al. 2010). The majority of the Hungaria asteroids are members of the Hungaria Hirayama family, i.e. they are remnants of a collisional event and originate from the same body.

The dynamical properties of the Hungaria family suggest it being a primitive population without outside intruders. The isolated nature of Hungaria asteroids among the asteroid population makes them a formidable sample of different processes affecting the MBA population, such as space weathering and Yarkovsky and YORP effects, and provides a dynamical constraint in modeling the evolution of the Solar System. The isolated nature of Hungarias presents a separate assessment of the significance of different mechanisms affecting the rotation of asteroids and binary formation without needing to take into consideration neither the entire main-belt asteroid population nor planetary encounters. Furthermore, the isolation from resonance areas can also be used to assess the significance of planetary encounters on, e.g., rotation rate distributions compared to other asteroid populations (such as NEAs) subject to planetary encounters.

The Hungaria asteroids have been observed to have an excess of slow rotators with an otherwise flat rotation rate distribution, which bears similarity to the NEA

[1] `ftp://ftp.lowell.edu/pub/elgb/astorb.html`

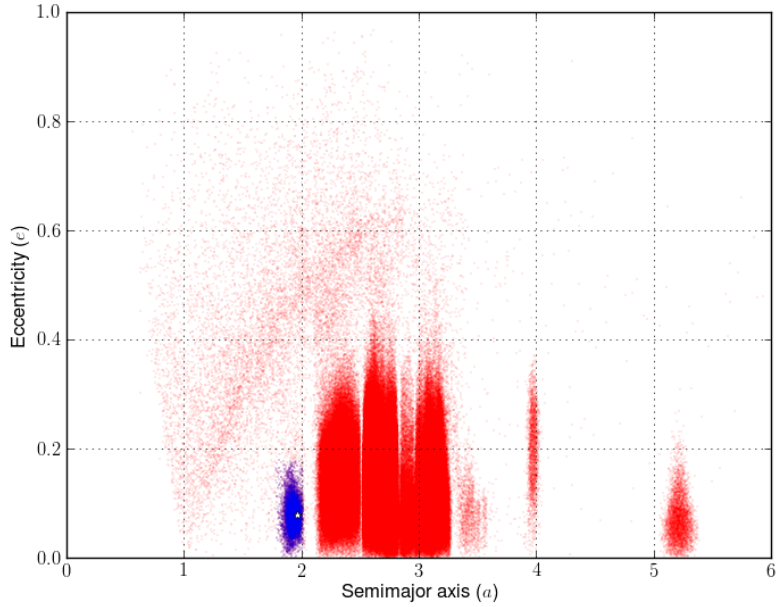

Figure 1.4: The semimajor axis-eccentricity plot of known asteroids with $a < 6$ AU. Hungaria asteroids are marked with blue. The white spot in the blue population marks the place of the asteroid (39420) 2084 T-2. The source of data is the ASTORB database[1].

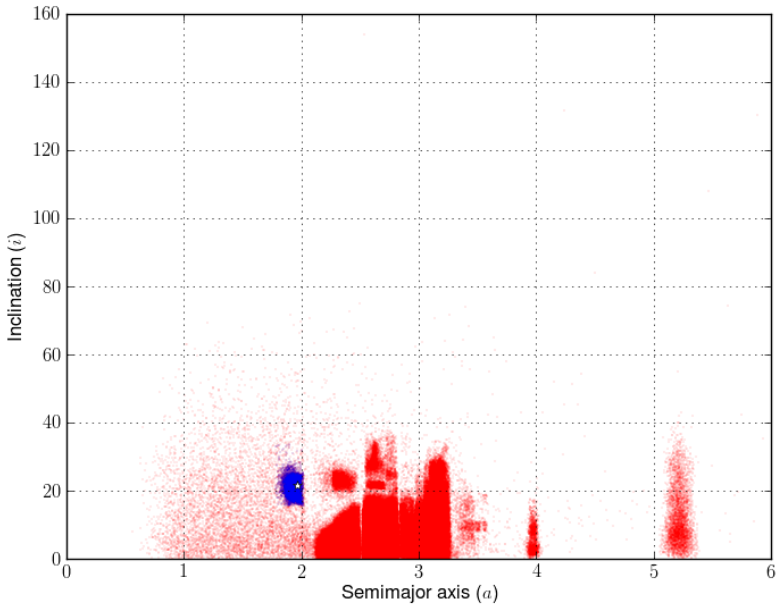

Figure 1.5: The semimajor axis-inclination plot of known asteroids with $a < 6$ AU. Hungaria asteroids are marked with blue. The white spot in the blue population marks the place of the asteroid (39420) 2084 T-2.

Semimajor axis	a	1.9612630 AU	1.1E-8 AU
Eccentricity	e	0.0788866	8.4E-8
Inclination	i	21.51499°	1.1E-5°
Longitude of the asc. node	Ω	187.51263°	1.3E-5°
Argument of the perihelion	ω	317.70817°	5.8E-5°
Mean anomaly	M	83.51249°	5.5E-5°

Table 1.1: Orbital elements of (39420) 2084 T-2 for the standard epoch November 4.0 2013 (MJD 56393). Values are obtained from the Ephemerides of Minor Planets for 2013 (Shor et al. 2012) and error estimates from the ASTDyS site[2].

rotation rate distribution. The Hungarias are also reported to generally have high albedos (Warner et al. 2009b).

1.4 The asteroid (39420) 2084 T-2

The asteroid (39420) 2084 T-2 was discovered on the 29th of September 1973 at Mount Palomar observatory during the Second Trojan survey by C. J. van Houten, I. van Houten-Groeneveld, and T. Gehrels (MPC 23291). It is a Hungaria population asteroid with orbital elements presented in Table 1.1. The location of the asteroid (39420) 2084 T-2 among the general asteroid population is shown in Fig:s 1.4 and 1.5.

Infrared observations from the WISE satellite suggest a diameter of 1.8 ± 0.2 km and a visual geometric albedo of 0.5 ± 0.1 (Masiero, private communication). These parameters classify the asteroid into the previously defined category of small asteroids.

The asteroid (39420) 2084 T-2 was observed in the statistical TALCS survey (Masiero et al. 2009) where it proved to be of particular interest in its own way.

[2] `http://hamilton.dm.unipi.it/astdys/`

The various values found for the asteroid (39420) 2084 T-2 were: amplitude of brightness $A = 0.8^m$, period $P = 105$ h $\pm$ 21 h and colour g'-r' = 1.913 $\pm$ 0.050. The combination of high amplitude and a long rotation period initially suggested the possibility of the asteroid being a binary or a contact binary asteroid.

1.5 Aim of the thesis

The following two specific goals for this thesis may be formulated. The first objective of this work is to review explanations for the rotation rate distributions of asteroids with different sizes and mechanisms affecting the rotation rate of asteroids. The second objective is to determine the period and convex shape model of the slowly rotating small Hungaria asteroid (39420) 2084 T-2.

The work is organized in a manner described below. In this chapter the reader has been introduced to asteroids and their rotation. Chapter 2 discusses the methods of observation and classification of asteroid rotation and physical processes affecting the asteroid rotation. Chapter 3 describes various methods used to obtain the results for this work. Consequently, the results are presented in chapter 4, and are further discussed in chapter 5. Chapter 6 comprises the concluding remarks of the thesis.

2. Rotation of asteroids

The existing techniques for asteroid period determination require substantial amounts of observations for an unambiguous result. Current (Catalina Sky Survey, Pan-STARRS 1) and future (e.g., Large Synoptic Survey Telescope) asteroid surveys provide only sparse photometric data as asteroid discovery is the primary objective of these surveys.

Comparing to the frequently performed survey observations with only a few observations at a time, dedicated long photometric series are rare. Especially, periods of slowly rotating asteroids are difficult to obtain. An unambiguous period usually requires a complete coverage of the rotational phase, which in case of slowly rotating asteroids is not achievable due to natural diurnal and annual cycles.

The difficulty of defining the rotational period of slowly rotating asteroids acts as a bias factor against them. The failure to obtain slow periods in combination of successful determinations of fast rotators results in excess of fast rotators in the known population in a general case during surveys where observational time is initially distributed evenly between asteroids. Since the determination of period of slow rotators is often just preliminary, the true distribution of slow rotators is subject to speculation.

2.1 Rotation of rigid bodies

An ideal rigid body is a combination of point masses with constant distances between them. A rigid body has intrinsic rotational kinetic energy. The possible sources for that energy are introduced in section 2.3.

Strictly speaking, all asteroids are not rigid bodies. However, it is reasonable to approximate asteroids to be rigid bodies on a short scale, e.g. during a random single rotation around its axis. The reason for this is that the changes in the shape of an asteroid and ejection of matter due to constant external forces happen on a much longer time scale than a single rotation period, which is a reasonable time scale to investigate the rotation process. Random events, such as ejection of matter and change of angular momentum due to collisions happen infrequently on the time scale of a single rotational period.

Six degrees of freedom are required to constrain the place and orientation of the rigid body in the inertial coordinate frame. Three degrees are constrained by the location of the centre of mass of the body in the inertial coordinate frame. The three remaining degrees of freedom give the orientation of the rigid body. A common way to describe the orientation of the rigid body is by using the so called Euler angles (Koskinen & Vainio 2010). The schematic drawing of conversion from the inertial coordinates to the rotating body coordinate as well as the location of Euler angles φ, θ and ψ is presented in Fig. 2.1.

The transfer matrix from the inertial coordinate system to the possibly non-inertial coordinate system of the rigid body is (Koskinen & Vainio 2010)

$$R(\varphi,\theta,\psi) = \begin{pmatrix} \cos\psi\cos\varphi - \cos\theta\sin\varphi\sin\psi & \cos\psi\sin\varphi + \cos\theta\cos\varphi\sin\psi & \sin\theta\sin\psi \\ -\sin\psi\cos\varphi - \cos\theta\sin\varphi\cos\psi & -\sin\psi\sin\varphi + \cos\theta\cos\varphi\cos\psi & \sin\theta\cos\psi \\ \sin\theta\sin\varphi & -\sin\theta\cos\varphi & \cos\theta \end{pmatrix}$$

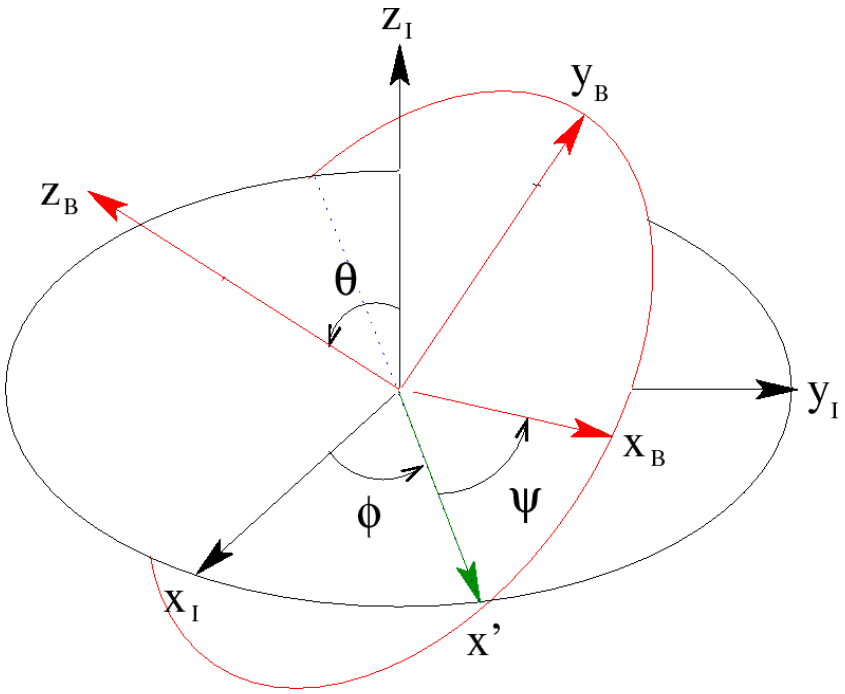

Figure 2.1: A scheme of Euler angles θ, φ and ψ. The origo point of the inertial and the body coordinate system is the same. The direction of the node is marked by x', the inertial coordinate system by x_I, y_I and z_I and the intrinsic body coordinate system by x_B, y_B and z_B[1].

and the transfer of coordinates is derived as

$$\{y\} = R(\varphi, \theta, \psi)\{x\}$$

where $\{x\}$ and $\{y\}$ are the inertial coordinate system and the body coordinate system respectively.

In the case of principal-axis rotation, the physical meaning of Euler angles is graphic (Kaasalainen 2001). The angle $\psi(t)$ corresponds to the rotation of the body around the rotation axis, the angle $\varphi(t)$ gives the extent of the precession of the rotation axis, while the angle $\theta(t)$ gives the extent of the nutation of the rotation axis. In the case of non-principal-axis rotators, the meaning of the angles is the same, but the body does not return to initial positions with respect to the inertial coordinate frame.

[1]The picture is from `http://hepweb.ucsd.edu/ph110b/110b_notes/node31.html`

The rotation state of an asteroid can be either relaxed or excited. The relaxed rotation state corresponds to the lowest energy state of the system while in an excited state, the rotation of an asteroid has been deflected from the relaxed state. Usually, for asteroids, the relaxed state is the principal axis rotation but there are some exceptions (Harris 1994).

The angular momentum vector $\vec{L}$ is defined as

$$\vec{L} = \hat{I}\vec{\omega}$$

where $\hat{I}$ is the inertia tensor and $\vec{\omega}$ is the angular velocity vector.

The inertia tensor $\hat{I}$ combines the terms of moments and products of inertia:

$$\hat{I} = \begin{pmatrix} I_{11} & I_{12} & I_{13} \\ I_{21} & I_{22} & I_{23} \\ I_{31} & I_{32} & I_{33} \end{pmatrix}$$

where each term I_{ik} is

$$I_{ik} = \sum m(y_j^2 \delta_{ik} - y_i y_k)$$

and where δ_{ik} is the Kronecker delta and y_{ijk} are coordinates of point masses m comprising the rigid body.

Because the matrix is symmetric, the inertia tensor can be diagonalized with a rotation of coordinates. Then the inertia tensor becomes

$$\hat{I} = \begin{pmatrix} I_1 & 0 & 0 \\ 0 & I_2 & 0 \\ 0 & 0 & I_3 \end{pmatrix}$$

The elements on the main diagonal are termed principal moments of inertia and the coordinate system where the inertia tensor is valid is called the main axis coordinate system. If any two main moments of inertia are equal then the rigid body is a symmetric top. In the general case where the main moments of inertia

are all different, the rigid body is an asymmetric top. In the case of the principal-axis rotation, the main rotation axis is aligned with the main moment of inertia possessing the highest value.

After introducing the basic concepts of rigid-body dynamics, the next step is to apply them to the topic of this study, i.e. asteroids, and particularly non-principal-axis rotators as an interesting example. It is evident from lightcurves that the majority of asteroids have only a single rotation period, which implies that the rotational axis of asteroids corresponds to the principal main moment of inertia.The shape of asteroids is hardly ever symmetric or spherical. Therefore, it is fair to state that all asteroids are asymmetric tops, i.e. all three moments of inertia are not equal. Thus, all asteroids experience some level of torque-free precession. For principal-axis rotators precession and nutation are slow compared to their rotation. For non-principal-axis rotators, the precession is embedded in the rotation process during a single rotation around its axis. This is the reason for the fact that non-principal-axis rotators never return to the same position with respect to the inertial coordinate frame after a single revolution.

When an asteroid is in an excited state, i.e. a non-principal-axis rotator, there are two modes of rotating – the long and short axis modes, i.e LAM and SAM (Samarasinha & A'Hearn 1991). LAM asteroids rotate around the longest axis and oscillate around the shortest one, while SAM asteroids act in the opposite way. The level of excitation for LAM asteroids is higher than for SAM asteroids, as it requires more energy and time to return to the relaxed state in the long-axis mode. In addition, there are also temporary transitional asymptotic rotation modes (Vokrouhlický et al. 2007).

In order to obtain a rotation model of a non-principal-axis rotator it is necessary to solve an inverse problem requiring the minimization of the function χ^2, i.e. the sum of squares of residuals from observations and the fitted model (Pravec

et al. 2005):

$$\chi^2(\lambda_L, \beta_L, \varphi_0, \psi_0, P_\psi, P_\varphi, I_{sym}, I_{ant}) = \sum_i (o_i - m_i)^2$$

where λ_L and β_L are latitude and longitude of the angular momentum vector L, φ_0, ψ and θ are Euler angles, P_ψ is the rotation period, P_φ is the precession period, and $I_{sym} = (I_1 + I_2)/2$ and $I_{ant} = (I_1 - I_2)/2$ are symmetric and asymmetric inertia axis values respectively.

Some of these values can be obtained from lightcurves, and the rest can be solved iteratively. In the following, a robust model for the non-principal-axis rotation is presented. The derivations follow Landau & Lifshitz (1965), Koskinen & Vainio (2010), Samarasinha & A'Hearn (1991) and Kaasalainen (2001).

It is possible to define the rotation period P_ψ, precession period P_φ and nutation period P_θ with known values of main moments of inertia $I_1 < I_2 < I_3$ as well as total kinetic energy E and absolute value of the angular momentum vector $L = |\mathbf{L}|$.

The starting point is writing Euler's equations, i.e. equations of motion of a rotating rigid body with no outside torques:

$$I_1 \frac{\mathrm{d}\omega_1}{\mathrm{d}t} - \omega_2\omega_3(I_2 - I_3) = 0 \tag{2.1}$$

$$I_2 \frac{\mathrm{d}\omega_2}{\mathrm{d}t} - \omega_3\omega_1(I_3 - I_1) = 0 \tag{2.2}$$

$$I_3 \frac{\mathrm{d}\omega_3}{\mathrm{d}t} - \omega_1\omega_2(I_1 - I_2) = 0 \tag{2.3}$$

where ω_i is the rotation velocity along the respective moment of inertia. The equations of conservation of energy and angular momentum give

$$I_1\omega_1^2 + I_2\omega_2^2 + I_3\omega_3^2 = 2E \tag{2.4}$$

and

$$I_1^2\omega_1^2 + I_2^2\omega_2^2 + I_3^2\omega_3^2 = L^2 \tag{2.5}$$

Now solving ω_1^2, ω_2^2 and $\mathrm{d}\omega_2/\mathrm{d}t$ from the previous equations:

$$\omega_1^2 = \frac{(2EI_3 - L^2) - I_2(I_3 - I_2)\omega_2^2}{I_1(I_3 - I_1)} \tag{2.6}$$

$$\omega_3^2 = \frac{(L^2 - 2EI_1) - I_2(I_2 - I_1)\omega_2^2}{I_3(I_3 - I_1)} \tag{2.7}$$

$$\frac{\mathrm{d}\omega_2}{\mathrm{d}t} = \omega_1\omega_2\frac{I_3 - I_1}{I_2} =$$

$$= \frac{\sqrt{((2EI_3 - L^2) - I_2(I_3 - I_2)\omega_2^2)((L^2 - 2EI_1) - I_2(I_2 - I_1)\omega_2^2)}}{I_2\sqrt{I_1 I_3}} \tag{2.8}$$

It must be noted that by convention, $2EI_1 < L^2 < 2EI_3$, and the stable solutions (LAM and SAM rotations) appear when L^2 are asymptotically approaching either of the extreme points.

By separating the variables, the time function $t(\omega_2)$ can be obtained. First, the new variables τ, s and k^2 are introduced:

$$\tau = \mathrm{d}t\sqrt{\frac{(I_3 - I_2)(L^2 - 2EI_1)}{I_1 I_2 I_3}}; \quad s = \omega_2\sqrt{\frac{I_2(I_3 - I_2)}{2EI_3 - L^2}}$$

$$k^2 = \frac{(I_2 - I_1)(L^2/2E - I_3)}{(I_1 - I_3)(I_2 - L^2/2E)}$$

Now $\omega^2 = 0$ when $t = 0$ is assumed.

First, ω is replaced with s as an integrable in equation 2.8:

$$\frac{\mathrm{d}s}{\mathrm{d}t} = \sqrt{\frac{(2EI_3 - L^2)I_2}{(2EI_3 - L^2)I_2}}\sqrt{\frac{(L^2 - 2EI_1)(I_3 - I_2)}{I_1 I_2 I_3}}\sqrt{(1 - s^2)(1 - k^2 s^2)} \tag{2.9}$$

Then, dt is replaced with τ:

$$\tau = \int_0^s \frac{\mathrm{d}s}{\sqrt{(1-s^2)(1-k^2s^2)}} \tag{2.10}$$

The solution to this is the Jacobi elliptic integral $s = \mathrm{sn}\ t$. Now the angular velocities as a function of time for all three main moments of inertia can be declared with the help of Jacobi elliptic functions $\mathrm{sn}\ t$, $\mathrm{cn}\ t = \sqrt{1-\mathrm{sn}^2\ t}$ and $\mathrm{dn}\ t = \sqrt{1-k^2\mathrm{sn}^2\ t}$:

$$\omega_1 = \sqrt{\frac{2EI_3 - L^2}{I_1(I_3 - I_1)}}\mathrm{cn}\ t \tag{2.11}$$

$$\omega_2 = \sqrt{\frac{2EI_3 - L^2}{I_2(I_3 - I_2)}}\mathrm{sn}\ t \tag{2.12}$$

$$\omega_3 = \sqrt{\frac{L^2 - 2EI_3}{I_3(I_3 - I_1)}}\mathrm{dn}\ t \tag{2.13}$$

To get the rotational period, one must take the closed integral. For ellipsoid integrals the solution is $4K(k)$, where

$$K(k) = \int_0^1 \frac{\mathrm{d}s}{\sqrt{(1-s^2)(1-k^2s^2)}} = \int_0^{\pi/2} \frac{\mathrm{d}x}{\sqrt{1-k^2\sin^2 x}}$$

and finally the rotational period is obtained by substituting τ with t (the vector returns to the same position with respect to the main axes of the body, and not with respect to the inertial coordinate frame). This is by definition, the rotation period P_ψ:

$$P_\psi = 4K(k)\sqrt{\frac{I_1I_2I_3}{2E(I_1 - I_3)(I_2 - L^2/2E)}} \tag{2.14}$$

$$P_\varphi = 2\pi\frac{P_\psi}{2\int_0^{P_\psi/2}\dot{\phi}\mathrm{d}t} \tag{2.15}$$

$$P_\theta = \frac{P_\theta}{2} \tag{2.16}$$

where

$$\dot{\phi} = L(\frac{1}{2I_1} + \frac{1}{2I_1} + \cos 2\psi(\frac{1}{2I_1} - \frac{1}{2I_1}))$$

These equations are valid for both LAM and SAM non-principal-axis rotators. The remaining problem is to estimate the principal moments of inertia. By normalizing I_3 and the longest axis c to 1, other moments of inertia can be derived from assuming an asteroid being an ellipsoid and estimating the length of their axes:

$$I_1 = \frac{b^2 + 1}{a^2 + b^2}; \qquad I_2 = \frac{a^2 + 1}{a^2 + b^2}$$

The model of non-principal-axis rotation has been applied to several asteroids (see Pravec et al. 2005).

2.2 Methods of observations of asteroid rotation and shape

The detection of asteroid rotation is essentially tied to their shapes. Only a few of the largest asteroids have a nearly spherical shape. Thus, period determinations should be combined with shape models, as erroneously determined periods result in false shapes and vice versa.

All various techniques used for observing asteroids are able to contribute in some way to resolving asteroid rotation rates and shapes. These observational techniques are presented in the subsection below.

2.2.1 Photometric observations

Photometric observations include calculating the incoming flux of photons from specified bodies and calibrating it with respect to both the background noise level and an absolute reference system. The alternative term for this method is disk-integrated photometry, because the value of exposed pixels is added, i.e. integrated over the disk for measurement of total brightness. This is opposed to disk-resolved photometry (see subsection 2.2.2) which includes the asteroid silhouettes and brightness variations across the projected surface area.

From the point of view of disk-integrated observations, asteroids are point sources, i.e., their angular size is much smaller than the angular resolution of the telescope. Due to astronomical seeing and imperfectness of the telescope optics the image of a point source is spread between several pixels. The method used to obtain the intensity and, consecutively, the magnitude value is called aperture photometry. The background noise is subtracted from the exposed pixels, the remaining values of which are integrated over the disk.

In order to obtain the absolute values for the asteroid magnitudes, the standard star calibration must be performed. Standard stars are non-variable stars which are calibrated to an absolute magnitude scale. In what is known as relative photometry, several standard stars at different zenith angles are observed each night. The differences between observed and real magnitudes are interpolated as the function of air mass (secant of the zenith angle). The observed asteroid magnitudes are then adjusted according to their respective air masses.

Another method, known as differential photometry, requires a standard star to be in the same field of view as the observed object. For asteroids, which move quickly comparing to stars, it is not always possible. Frequently, there are no standard star observations or calibrations whatsoever for asteroid observations, e.g. when asteroid observations cover the entire rotational phase during one night.

Though applied on the same scale, the asteroid magnitude system differs from that of stars. The brightness of asteroids varies depending on their phase angle, i.e., an angle between the Sun, the asteroid and the observer. The asteroid is at its brightest when the phase angle is zero, i.e., at opposition. The brightness decreases steeply within several angles from opposition. After that, the decrease happens much slower, behaving almost linearly with the growth of the phase angle. While the general shape of the slope is similar for all asteroids, with respect to details, it is nevertheless unique for each asteroid.

To address the dependence of the brightness of asteroids on the phase angle, an empiric three parameter system (Muinonen et al. 2010) has been introduced to be able to calculate any asteroid's magnitude at any phase angle. These three parameters are a result of a linear least-squares fit to observations, which are consequently transformed into the final parameters. Of these parameters, one is the magnitude at opposition while the two others are shape parameters of the slope.

Photometric observations of asteroids comprise the main bulk of asteroid rotation data. Radar data is second in importance. At the moment other data obtained by alternative methods is complementary.

Ground-based photometric observations of asteroid lightcurves do not typically require large telescopes and can therefore be performed rather cost-effectively. On the other hand, a lot of observation time is required to acquire a sufficient amount of lightcurve data for a satisfactory analysis of the rotational period. A rough estimate, however, can be obtained from an observation set with a span of only a few nights. For asteroids with a rotational period less than 10 h, which comprise a significant bulk of resolved periods, several nights usually enough for a satisfactory analysis.

Some photometric observations of asteroids are by-products of astrometric observations. These observations usually have larger uncertainties than dedicated photometry due to shorter exposure time required for astrometry, resulting in a lower

signal-to-noise ratio and larger errors. A large portion of asteroid data comes from the NEA surveys which emphasize astrometric precision and coverage of sky. During these surveys, no standard star calibrations, and not even standard photometric system filters are used.

The inverse methods of obtaining rotational periods and shapes of asteroids from photometric lightcurves are presented in chapter 3.5. Photometric data usually permits resolving a global convex model within which the asteroid is contained.

A high amplitude of an asteroid lightcurve is an indirect indication of an elongated shape of the asteroid or a binary / contact-binary system. Multiple periods can also indicate a binary object as well as an asteroid rotating in a tumbling state. With a help of adaptive optics it is possible to distinguish binary (Merline et al. 1999) and even ternary (Marchis et al. 2005) components directly in the main belt. Binaries are predicted to comprise a significant portion of main-belt asteroids (according to Warner et al. (2009b) ca. 15 % of NEAs and Hungarias are binary systems).

Direct determinations of binaries are nevertheless rare. Certain properties in photometric lightcurve such as flat brightness with steep minima point directly to the asteroid being a binary. Several such asteroids have been found and a binary model for them has been constructed (Pravec et al. 2006).

Other, less prominent indirect signatures in the lightcurve fit may also suggest an asteroid to actually be a binary during lightcurve inversion (Ďurech & Kaasalainen 2003). These signatures are revealed when compared to synthetic lightcurves produced by the inverted convex shape models. These signs are tight turns and steeper slopes compared to synthetic fits of respectable convex shapes in addition to large flat areas on elongated model shapes.

Several asteroid photometric lightcurve databases exist for different purposes. The most important ones are presented below.

The Uppsala Asteroid Data Base (Magnusson et al. 1994) previously included all available dedicated asteroid photometric data of asteroids. It is now succeeded by the Asteroid Photometric Catalogue maintained at the University of Helsinki[2]. Some photometric observations are also published by the Minor Planet Center.

The data published in the annual volume of Ephemerides of Minor Planets (Shor et al. 2012, prepared by B. Warner, A.W. Harris and P. Pravec) is compiled from several sources and includes the data for those of asteroids for which the data exists, the main source is the Asteroid Lightcurve Database (LCDB, Warner et al. 2009a). The data sets include the rotational period, the observed magnitude amplitude and reliability parameter U; the alternative rotational period values for some asteroids; a primary and secondary period as well as the primary amplitude of asteroid binary systems; the period of binary asteroids as well as the semimajor-axis of the secondary around the primary; data on tumbling asteroids; the rotation pole orientation of asteroids. The period data exists for 4942 asteroids and binary data for 148 asteroids as of 2013.

The Database of Asteroid Models from Inversion Techniques (DAMIT, Ďurech et al. 2010) includes the data on asteroid periods, convex models of shapes from lightcurve inversion and asteroid shape silhouettes deducted from occultation images. Convex shape models exist for 347 asteroids as of May 2013.

The previously mentioned databases generally contain high-precision photometry. The photometric data from the Minor Planet Center has been combined with the Lowell Observatory ASTORB database[3], an astrometric database of over half a million asteroids which also contains some photometric data as a by-product of astrometric data. This data is of significantly lower precision, but estimates for the magnitude and slope of asteroids can be obtained (Oszkiewicz et al. 2011).

[2] `http://asteroid.astro.helsinki.fi`

[3] `ftp://ftp.lowell.edu/pub/elgb/astorb.html`, maintained by E. Bowell and L. H. Wasserman

The database of asteroid rotation pole orientations has been created at the Uppsala University and is currently maintained at the University of Poznań (Kryszczyńska et al. 2007). It contains pole solutions for around two hundred asteroids. The previously mentioned Lowell database is also used to derive estimates on the pole orientation of all asteroids (Bowell et al. 2013).

2.2.2 Disk-resolved images

The simplicity of disk-integrated photometry does not permit to take into consideration brightness variations, limiting the range of possible solutions. In a disk-resolved image, the silhouette of the asteroid, its surface features as well as possible albedo variations may be observed.

For some asteroids, the shapes and albedo variations may be viewed directly from high-precision telescopes with adaptive optics. By combining several observations it is possible to construct a realistic three-dimensional model of an asteroid. Current ground-based facilities allow such observations for only a handful of large and near asteroids. However, proposed next generation observational facilities such as the JWST or E-ELT will be able to provide angular resolution of approximately 0.01", increasing the number of observable asteroids.

Disk-resolved images are also taken during the *in situ* missions. The notable spacecraft flybys include observations of (951) Gaspra and (243) Ida by Galileo, (253) Mathilde and (433) Eros by NEAR Shoemaker, (25143) Itokawa by Hayabusa (Spjuth 2009, and references therein), and, most recently, (3) Vesta and (1) Ceres by Dawn. During these missions, also surface features of asteroids could be observed at various distances. The general results confirmed by disk-resolved and radar images are that larger asteroids have nearly spherical shapes close to hydrostatic equilibrium while small and medium-size asteroids tend to have major irregularities, such as concavities and sharp edges.

2.2.3 Occultation images

Asteroids occasionally transit in front of stars covering them at the event. The transits and eclipses of stars are called occultations. Due to different observational geometries from various observatories, the duration of occultations varies depending on the location of observatories. By combining observations of brightness change of the background star as function of time along the occultation path, which can comprise certain parts of an entire continent, it is possible to resolve the contours, and sometimes even concavities, of the observed asteroid (Lucas 2004). Due to the small size of asteroids, the span of occultation observations is tens of seconds at maximum.

The occultations of asteroids can be predicted and observations coordinated in advance. The combined result is however only a two-dimensional projection of the shape at a random moment. In order to construct a three-dimensional model relying exclusively on occultation image data, one must observe several transits of the same asteroid at different geometries.

This observational technique is suitable solely for rather large asteroids at a limited time and a limited part of the Earth. Though occultations can be predicted, they occur randomly and infrequently for any given asteroid. In addition, it is a complicated procedure requiring coordination of different observatories, and therefore is not suitable as a primary source of information for asteroid shape determination. On the other hand, occultation observations are possible to perform also with fairly small telescopes.

A method combining lightcurve inversion, occultation images, and disk-resolved images has been recently developed (KOALA, Carry et al. 2012).

2.2.4 Infrared images

Due to the Earth's atmospheric restrictions, only several narrow observational wavelength bands exist for infrared imaging. Therefore, spaceborne missions are optimal for infrared observatories. As the wavelength of thermal radiation lies in the infrared area of the spectrum, the infrared instrumentation must be cooled close to absolute zero to maintain sufficient signal to noise ratio. Currently, it is possible to maintain autonomous cooling system in spaceborne observatories for only a few years. All these factors make it more challenging to obtain observations in the infrared band in comparison to many other wavelengths.

The most significant role of infrared imaging of asteroids is that in combination with photometric observations it permits solving their diameter and geometric albedo separately. Photometric observations alone are able to resolve only the combined value $D^2 \cdot A$, where D is the diameter of an asteroid and A its geometric albedo (Harris & Lagerros 2002). The values can be separated by comparing a thermal model to the measured scattered and emitted radiation from the asteroid. This is possible because thermal emission and optical reflectivity act in opposite ways as a function of surface albedo: reflectivity increases and emission decreases with growing albedo, and vice versa. In order to construct a plausible infrared model, the absolute magnitude H of the asteroid must be well known. It should be mentioned that the thermal models in use are simple. For example, the models assume a spherical shape for an asteroid, which can be justified only for certain large asteroids.

In addition, the infrared imaging of asteroids can be used to assess the scale of effect of the Yarkovsky or YORP thermal effects on asteroid rotation[4].

[4] `http://osiris-rex.lpl.arizona.edu/?q=node/521`. OSIRIS-REX is an upcoming sample return mission to asteroid 1999 RQ_{36}

2.2.5 Radar observations

Two fundamental values obtainable from the radar observations are the distance and the velocity of the asteroid. The former is observed as the time delay of the outgoing and the incoming radar impulses while the latter is calculated from the observed Doppler frequency. A quantitative estimate for the surface roughness can also be derived from the radar echo. This is another independent, and convenient inverse method to define a three-dimensional shape model of the asteroid, by observing from different geometries.

Radar observations are able to target NEAs during close approaches to the Earth, as well as some MBAs near their opposition. By the end of 2012, 132 MBAs and 353 NEAs, as well as 16 comets have been observed by radar. Due to the combination of necessary requirements, i.e. a large antenna and relatively small distance to a body being observed, radar astronomy can be performed by only a handful of large radio telescopes comparing to the large amount of optical telescopes suitable for conducting usual astrometry and photometry. In particular, MBAs can be observed only by the Arecibo radio telescope, where only limited observational time is allocated to asteroid radar astronomy (Ostro et al. 2002).

The advantage of the radar observations is their great precision in all aspects. In astrometry, radar ranging for NEAs has greatly improved orbit predictions for the observed bodies because observational errors in radar observations are so small. Radar observations also play an important role in NEA shape modelling, e.g. radar observations are currently responsible for resolving for over 85 % of known NEA binaries[5].

Although radar observations are of great precision, they are nevertheless much more limited than e.g., photometric observations by technical feasibility and therefore are not suitable for a systematic survey such as TALCS.

[5] `http://echo.jpl.nasa.gov/~lance/binary.neas.html`

2.3 Despinning mechanisms of small asteroids

The cloud of primordial bodies had the initial moment of inertia dispersed between its members. Thus, every primordial body in the main asteroid belt had had an initial rotation rate. However, not a single asteroid in the main belt has experienced any effect on their rotation, as even the largest unfragmented bodies have undergone numerous collisions and, as a result, are filled with craters. Thus, there is no knowledge on the initial rotation distribution of the asteroid belt, and the time scales of the mechanisms affecting the rotation are very short compared to the age of the Solar System.

Different mechanisms affect the alteration of the rotation rates of celestial bodies. They can be divided into random events and constant forces.

2.3.1 Impacts and collisions

The impact-driven mechanisms that are responsible for alteration of the rotational period of asteroids are the angular momentum drain and catastrophic collisions.

The angular momentum drain (Dobrovolskis & Burns 1984) occurs upon an impact as previously defined, where the smaller body (= the impactor) disintegrates but the larger body (= the target) does not. While the direction of the ejecta from the crater is distributed isotropically, the angular velocity of the target contributes to their speed. Thus, more ejecta moving in the direction of the rotation of the target escape the gravitational field of the body due to the boost, whereas more ejecta moving in the opposite direction fall back on the surface. Consequently, the target loses its angular momentum to the escaped ejecta.

The size of an asteroid beneath which no ejecta is returned back to the surface varies with the structure of asteroids. For monolithic (or “hard”) asteroids this boundary is ca. 39 km. For a structure, more representative for a typical asteroid, the boundary is calculated to be ca. 6 km. Therefore small asteroids are constantly

stripped of matter, and are never replenished.

The direct change of angular momentum (assuming rigid bodies) from impacting bodies is negligible (Pravec et al. 2005). In a situation where a very slowly rotating asteroid is on the verge of succumbing to a tumbling state, the influence of the impact may however be sufficient to trigger the non-principal-axis rotation.

The collisional time scale of asteroids in the main belt increasing with the ever diminishing amount of asteroids. In an evolved population, the collisional lifetime of asteroids is also a function of its size (Bottke et al. 2005). For instance, asteroids with a diameter of 1 m have an average collisional lifetime of 14 million years, a 1 km asteroid – 440 million years and 100 km asteroid – 34 billion years. Since the collisional timescale of largest asteroids is much higher than the age of the Solar System it implies that they are not disintegrated during their lifetime. Thus, impacts and collisions occur between small asteroids resulting in new bodies.

The dissipation of a larger body may happen either due to a catastrophic collision or decoupling of a single body due to centrifugal force exceeding the inner cohesion forces. The latter situation may occur when the YORP effect (see subsection 2.3.5) increases the rotational velocity of the body.

An asteroid collision is a catastrophic event where both counterparts of the event are significantly altered. Hirayama families were formed as a result of catastrophic collisions between two large asteroids, resulting in numerous smaller bodies, all with moments of inertia of their own. Some of the resulting bodies may remain close and form binary or even many-body systems.

The decomposition into a binary may further result in total separation of the two bodies. Such bodies can be recognized by integrating their orbital elements backwards. If the orbital elements at some point come within the Hill radius of each other then they most likely origin from the same parent body.

2.3.2 Depletion of gases

Main-belt comets are a recently discovered subcategory of comets. Found at the outskirts of the main asteroid belt, they are classified both as asteroids and as comets, as they satisfy somewhat vague criteria for both celestial body categories.

The current understanding of the main-belt comet phenomena indicates that the composition of these bodies is, in the same way as for comets, a so-called "dirty snowball". In a "dirty snowball", rocks and volatiles, such as water ice, are mixed. In addition, the surface of the main-belt comet consists of non-volatile components. The outbursts of gases from the main-belt comet are capable of altering the orbit and rotation rate of the body. Therefore, the depletion of gases would be short-termed due to the nature of main-belt comets. An impact exposes volatiles until the source is depleted or covered in regolith, effectively insulating the volatile area (Jewitt 2009).

For the short-periodic comet 103P/Hartley 2 the change of the rotational period due to outgassing has been measured directly (Samarasinha et al. 2011). Naturally, the cometary activity of comets coming closer to the Sun than the main asteroid belt is significantly higher. The rotational period of 103P/Hartley 2 increased by 0.5 h in one month.

For main-belt comets, this mechanism is, however, not as clearly applicable. For example, Husárik (2012) did not notice any change of rotational period on a plausible main-belt comet (596) Scheila after an outburst. Though there are fairly little results on the effect of cometary activity on rotation of main-belt comets, one possible conclusion could be that in order to have an effect on the rotational period, the cometary activity should be constant and abundant. Thus, short outbursts would have a negligible effect on the rotation rate of main-belt comets.

Some current asteroids may be depleted cometary nuclei. For some comets, the gaseous jets are able to maintain non-principal-axis rotation, which is currently

the case with e.g. 1P/Halley (Samarasinha & A'Hearn 1991, Harris 1994). The cometary activity ended long time ago may thus indirectly affect the rotation of asteroids in detectable ways for millions of years.

2.3.3 Gravitational encounters

The rotational period of a body can be changed during a close encounter with another celestial body due to the effect of exchange of angular momentum. The exchange of angular momentum happens through mutual tidal torques, especially if the body is irregularly shaped (Pravec et al. 2005). On such occasions, an asteroid can decline into a tumbling state.

Close bypasses in the main asteroid belt are not uncommon. However, due to the small masses of bodies, the effect of mutual gravitational encounters between asteroids is negligible. Nevertheless, in the case of planets the exchange of angular momentum is significant for the asteroid. Therefore, minor bodies can have their rotational rates altered significantly.

The main-belt asteroid population is primordial, i.e., it has not moved significantly from its initial birth place. The characteristic values of a dynamically hot (i.e., with a history of dynamical encounters with planets) populations are high inclinations and eccentricities, which the bulk of asteroids on stable orbits does not possess. As no planets are present in the region, it has been concluded that the change of rotational rate of main-belt asteroids cannot be the outcome of gravitational encounters with planets.

2.3.4 Binaries and spin-orbit resonances

The problem of distinguishing between single and binary asteroids in the main belt is not trivial. The resolution of current ground-based observatories is sufficient to

classify only some tens of asteroids as binaries[6]. More specific indications of binaries include steeper slopes and tighter turns than compared to a similar elongated object (Ďurech & Kaasalainen 2003). *In situ* missions are, on the other hand, infrequent and target only specific asteroids. Due to the conservation of the angular momentum, the rotation of a binary system around the common center of mass is slower than the rotation of a corresponding ordinary asteroid, assuming that the binaries are formed by breaking up larger asteroids.

Some observational features of an asteroid might indirectly indicate the possibility of the object being a binary. These features are large amplitudes in lightcurves and a long rotation period. The asteroid (39420) 2084 T-2 investigated in this thesis, bears both of these features. Moreover, significant colour and albedo variations as a function of time indicate a non-uniform composition of the body. If these variations are periodic then the body is likely to be binary because in some observational geometries a single body can hide these features.

A split of an ordinary asteroid into a binary asteroid is presented as a mechanism for slowing down the rotation of asteroids. According to Harris (2002), one possible source for slow rotation of asteroids is recently decoupled asteroids, where a transfer in rotational energy has occurred from the rotation around the axis into rotation of the secondary component around the primary component. The mechanism of Harris (2002) would then require for a secondary body to escape the binary system, leaving a single slowly rotating asteroid.

In addition, other forms of binary formations include recombination of ejecta as an aftermath of a collision (Michel et al. 2001) and, theoretically, capturing a smaller asteroid flying by. Indications of a recombination after a collision are a large secondary size compared to the primary and similar spectroscopic features of the

[6]IAU Central Bureau for Astronomical Telegrams: `http://www.cbat.eps.harvard.edu/minorsats.html`

surface layers. A capture of a flyby asteroid is highly unlikely for bodies with a small gravitational potential, such as asteroids.

A contact binary is a special case. Though it is technically a single object, its rotation dynamics are dominated by the fact that the mass is distributed in a binary manner. The prominent features of the shape are concavities in the middle and massive features at both ends.

2.3.5 Yarkovsky-O'Keefe-Radzievskii-Paddock effect

The Yarkovsky-O'Keefe-Radzievskii-Paddock (YORP) effect is a thermal torque mechanism which affects the angular momentum of a highly asymmetric body. The YORP effect occurs when the thermal photons from the body are dispersed anisotropically from an asymmetric body. Consequently, the momentum either increases or decreases, depending on the orientation of the rotating axis (Rubincam 2000). A simple model visualizing the YORP effect is presented in Fig. 2.2. As no asteroid is a perfect sphere or ellipsoid, the YORP effect generally applies to every asteroid. Actually, its scale is determined by the asteroid's size and shape, as highly irregularly shaped bodies are affected significantly more (Ćuk & Burns 2005). In the probable case of the asteroid being a rubble pile, the YORP effect may be responsible for accelerating the angular velocity of the body to the state of its disintegration (Vokrouhlický & Čapek 2002).

As the thermal emission is uneven, in addition to the principal-axis rotation the obliquity torque is also introduced. Should the principal-axis rotation slow down, the obliquity torques become significant. The YORP effect cannot slow down the rotation torque infinitely close to zero. The asteroid rotation can therefore decline to a tumbling state, or non-principal axis rotation (Vokrouhlický et al. 2007), a chaotic spinning motion. The lightcurves of tumbling asteroids usually include two or more distinguishable rotation frequencies (Pravec et al. 2005).

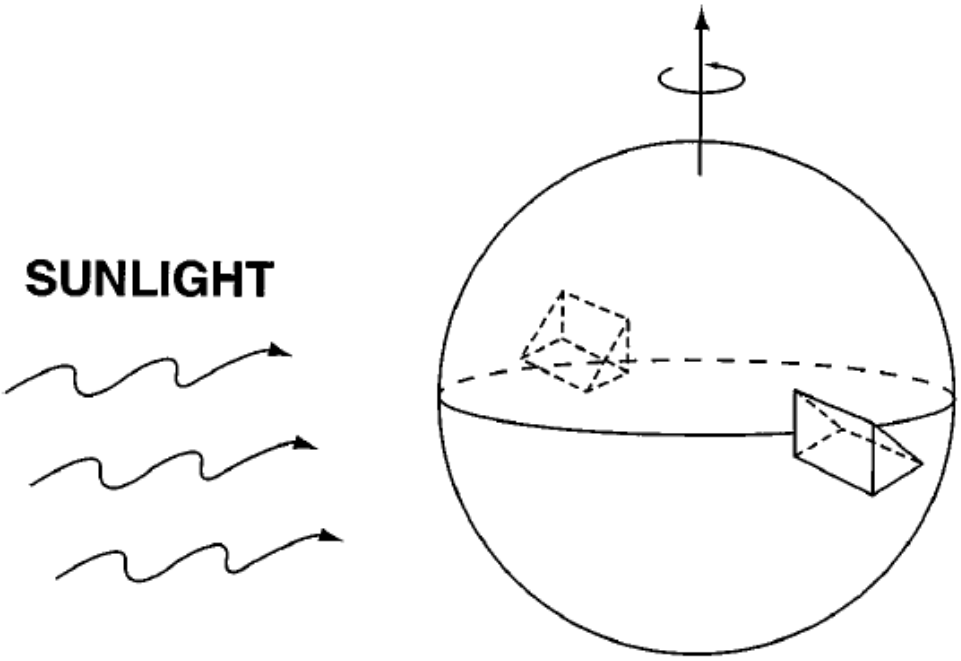

Figure 2.2: A simplified situation demonstrating the YORP effect from Rubincam (2000). The body absorbs light and later re-emits it. Due to an irregular shape, the thermal emission is dispersed unevenly, resulting in a net torque.

In the recent years, the YORP effect has been detected directly in several asteroid photometric lightcurves, e.g. for asteroids (1862) Apollo (Kaasalainen et al. 2007), (54509) YORP (Lowry et al. 2007) and (1620) Geographos (Ďurech et al. 2008). So far these asteroids have all been NEAs. The NEAs approach Earth at close distances which provides observers with opportunities of high resolution photometric lightcurves at various apparitions.

In addition to the preferential sets of observational geometry available for NEAs, small asteroids which are more affected by YORP, are better observed in the Earth's vicinity than in the main belt simply because they are absolutely brighter. Also, the strength of the YORP torque depends on the distance of the asteroid from the Sun. A reliable size distribution of main-belt asteroids exists for asteroids with absolute magnitude less than 15 (Gladman et al. 2009) which corresponds to the diameter of 2 - 6 km[7] (albeit there are several estimations which go beyond that limit based on observation samples). Also, around 93 % of kilometre-sized NEAs have already been discovered (Mainzer et al. 2011). For all the reasons mentioned above, the difference in rotational periods can be detected more easily in NEAs than MBAs.

While the YORP effect affects the rotation of asteroids in both directions, there are differences in these outcomes. While the spin down to a slow rotator or even a non-principal axis rotator is relatively fast, it takes a long time to spin the asteroid up back to a fast rotator. The reason for this discrepancy is that the tilt of the asteroid principal rotation axis grows with increasing angular velocity (Rubincam 2000) which, in turn, weakens the effect. For slowing down, however, there is no such mechanism.

Nevertheless, YORP acts as a mechanism for both spinning up and down the rotation rate of asteroids. This, in addition to the potentially disruptive nature of

[7] `http://www.minorplanetcenter.net/iau/lists/Sizes.html`

the fast rotation implies that the YORP effect is a major, if not primary, contributor among the different mechanisms responsible for the general excess of slow rotators.

Recent results (e.g. Cotto-Figueroa et al. 2013) indicate that YORP is not a constant force because "rubble pile" asteroids change their shape frequently. Small changes between bodies and particles comprising the "rubble pile" asteroid are possible due to the shattered or aggregated nature of the body. Even small changes in the shape of an asteroid can heavily affect the significance of the YORP force.

A special embodiment of the YORP effect, the binary YORP (BYORP) occurs in existing binary systems. It is assumed that the primary body is more or less spherical and is therefore unaffected by the YORP effect while the secondary body has an irregular shape, a prograde rotation and orbit direction. Thus, the net angular momentum of the system increases to the level that the secondary body might be ejected (Ćuk & Burns 2005). The lifetime of a binary system experiencing BYORP is much shorter than between possible planetary encounters, which is another plausible mechanism for binary decoupling.

The BYORP effect can also be responsible for the formation of binaries in some situations. For example, asteroids in the Hungaria region have no tidal encounters with planets. Thus, BYORP is thought to be the primary mechanism in binary asteroid formation in that area (Warner et al. 2009b) by shedding away materia after spinning up beyond the critical rotation rate of the "rubble pile". The shedded materia then regenerates into a secondary body which will begin to rotate around the primary body. A binary with a fast rotating primary is more likely to be produced by BYORP than by, e.g., the outcome of a catastrophic collision.

The YORP effect is size-dependent. The rotation-rate distribution of the largest asteroids follows closely the Maxwellian distribution while there clearly is an excess in both fast and slow rotators in the smaller asteroid populations (Pravec et al. 2002). The closely related Yarkovsky drift (Öpik 1951), a mechanism which

affects the orbits of asteroids resulting from a net force caused by emission of thermal radiation, is likewise size-dependent. The two mechanisms are closely bound in dispersing values of semi-major axes of asteroid Hirayama families (Vokrouhlický et al. 2006). The influence of the YORP effect is its ability to tilt the rotational axis in a manner most preferential for the Yarkovsky drift to take action. This mechanism is a major contributor to replenishing the NEA population by pushing the main-belt asteroids into mean-motion and secular resonance zones, and consequently, to the NEA area (Vokrouhlický & Farinella 2000).

2.4 Conducted surveys

An extensive review (Pravec et al. 2002) on asteroid rotation covered the rotational properties of asteroids with different sizes, their lightcurve amplitude distribution and rotational axis orientation distribution. Particularly, areas of dense population as well as completely empty areas have been found on the rotation-size diagram (see Fig. 1.3). Pravec et al. (2002) emphasized the importance of conducting an extensive unbiased lightcurve survey for small and mid-sized asteroids in order to clear up the picture. Two major surveys have been conducted ever since.

2.4.1 Thousand Asteroid Lightcurve Survey

The Thousand Asteroid Lightcurve Survey, or TALCS, (Masiero et al. 2009) was conducted with the Canada-France-Hawaii Telescope in September 2006. Being an untargeted survey, i.e., the survey included all asteroids which happened to appear in the observed portion of the sky, it included 828 main-belt asteroids. Of these only 278 asteroids had sufficient data for rotation period estimates. The diameters of these 278 asteroids range between 0.4 km and 10 km.

The follow-up observations of ten asteroids were conducted in 2008 using the

University of Hawaii 2.2-m telescope resulting in seven additional period estimates.

TALCS possibly detected six very fast rotators with a period of less than 2 h. These results, however, are not very reliable as these bodies have a small amplitude close to a level of background noise. If further confirmed, these observations would support the size-dependent strength theory of Solar System bodies (Holsapple 2007). The theory in question combines two mechanisms affecting the size-rotation distribution of asteroids – for asteroids smaller than 10 km in diameter the inner strength configuration of asteroids defines the upper limit of the rotation rate. For larger asteroids, gravitational forces begin to dominate. Therefore, the upper rotation frequency limit of 2 h for asteroids with a diameter larger than 10 km would necessarily imply their "rubble pile" structure because inner strength forces are insignificant for these bodies. A further assessment of these observations by Harris et al. (2012) refuted these results due to unreliable period estimates. Therefore, the model of Holsapple (2007) has not yet been confirmed.

In addition, TALCS results imply the period distribution resembling a Maxwellian with an excess of slowly rotating asteroids (see Fig. 2.3). The difference from previous results is the higher fraction of slowly rotating asteroids. This suggests that slow rotation periods are harder to obtain from observations, and that they represent a much more significant part of the asteroid population (especially at smaller sizes) than has been anticipated.

2.4.2 Photometric Survey for Asynchronous Binary Asteroids

The Photometric Survey for Asynchronous Binary Asteroids (Pravec et al. 2008), or BinAstPhotSurvey is an ongoing survey combining observations from various observatories around the world. The survey's primary objective is to detect binary asteroids. Lightcurves of around 300 asteroids with diameters less than 15 km were

collected during the survey.

The asteroids were specifically chosen for the survey based on their semi-major axis ($a < 2.5$ AU) and absolute magnitude ($H > 12^m$) which can be converted to the size of less than 10.2 - 17.6 km with a standard assumed geometric albedo of 0.18 ± 0.09 for inner main-belt asteroids. The choice has also been affected by the favourability of observing conditions.

The results of the BinAstPhotSurvey show a flat distribution for the rotation rate of asteroids with a diameter from 3 to 15 km with the exception of a significant excess in the slow rotator population. This result indicates a significant influence of the YORP effect on the small and middle-sized asteroid population. The survey raises a question on the nature of the size dependence of asteroids with diameters beneath 40 km on the YORP effect. The results themselves suggest that this dependence is negligible in the diameter range between 1 and 15 km.

2.4.3 Comparison of surveys

The difference in acquired rotation rate distributions in (Masiero et al. 2009) and (Pravec et al. 2008) is presented in Fig. 2.3.

The discrepancy of the results of Masiero et al. (2009) and Pravec et al. (2008) point to the difference in the data sets. Indeed, the TALCS was an untargeted survey spreading throughout the whole main asteroid belt while the BinAstPhotSurvey observed asteroids chosen in advance and in the inner main asteroid belt only.

The flatter distribution in Pravec et al. (2008) suggests the significance of the YORP effect on the rotating bodies. The observed bodies are situated in the inner main asteroid belt where the YORP effect has more influence than in the outer regions. Both surveys find an excess in very slowly rotating asteroids (rotation time over 30 hours) comparing to previously collected data. However, the distribution of slow rotators is more representative in (Masiero et al. 2009) as it is an untargeted

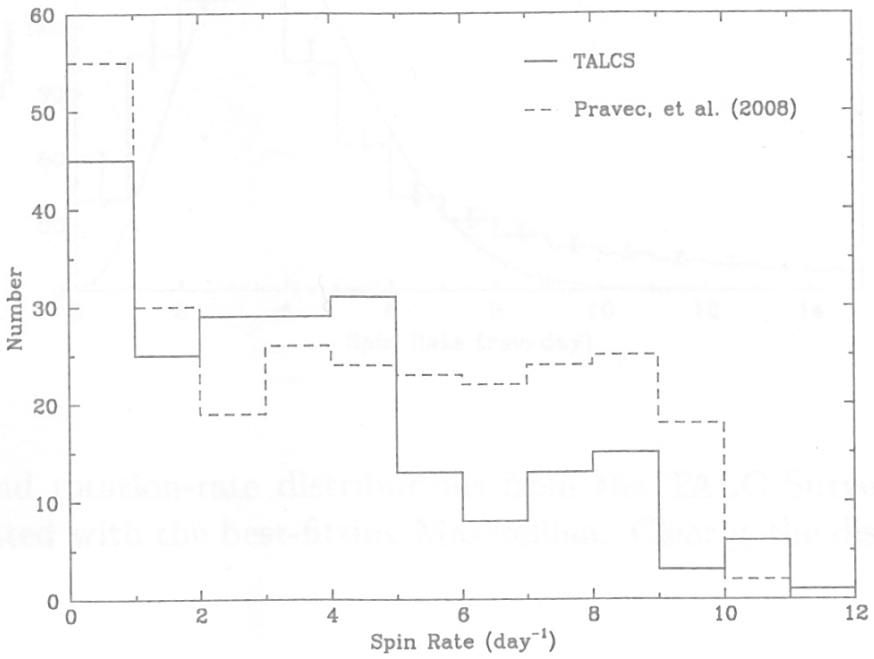

Figure 2.3: The differences between rotation rate distributions of Masiero et al. (2009, solid) and Pravec et al. (2008, dashed) of all observed asteroids. The plot is from Masiero et al. (2009). TALCS asteroids' diameter ranges from 0.4 km to 10 km, while the upper limit of diameters of the BinAstPhotSurvey is 15-17 km.

survey. The period determination for slow rotators must be improved further in order to obtain a more accurate distribution. The upper boundary for a precise rotational period determination was reported to be around 10 h.

A problem with surveys is that they treat all objects equally, although slowly rotating asteroids and asteroids with low amplitudes of the lightcurve always require more observations to reach a given accuracy threshold. The very essence of survey observations of a wide field is that the number of observations for each body is the same, while some asteroids clearly require more data than others.

The original survey observational plan of TALCS was designed for detecting asteroids with faster rotation periods, which left uncertainties in determining periods of the slow-rotating asteroids. Therefore, follow-up observations were needed to verify whether the period analysis of discovered slow rotators was statistically accurate.

3. Method

3.1 Observational characteristics

The first part of the data were the observations from TALCS (Masiero et al. 2009). TALCS was conducted primarily in the $g´$-band with $r´$-band observations on a single night. As the bulk of FU 1 observations is in the $r´$-band, it was decided to shift the TALCS $g´$-band data using the $g´$-$r´´$ colour index. The colour index from TALCS for asteroid (39420) 2084 T-2 is 1.913 ± 0.050.

As a follow-up of the TALCS survey, some observations of (39420) 2084 T-2 have been performed (Masiero et al. 2009). However, this data was not available for the current study due to hardware malfunction.

Follow-up observations of slowly rotating asteroids in TALCS (Masiero et al. 2009) were conducted by M. Granvik in 2009 (hereafter FU 1 observations). The observation campaign targeted certain slowly rotating asteroids already detected in the TALCS. The asteroid (39420) 2084 T-2 was one of the asteroids selected in the follow-up.

The observations were carried out using the University of Hawaii 2.2-m telescope (UH88) at the Mauna Kea Observatory.

The telescope began its operation in 1970 at the summit of Mauna Kea in Hawaii, USA. It was among the first of many professional observatories on that astroclimatically premium spot. The telescope has also pioneered imaging technology

implementing various forefront high-resolution cameras throughout the years. The telescope has been instrumental in expanding our knowledge on small bodies of the Solar System. In particular, the breakthrough in TNO observations has been made by observations conducted with the 2.2-m telescope since the 1990s.

The imaging instrument used for gathering photometry was the Tektronix 2048 x 2048 CCD-camera with a field of view of 7.5' x 7.5'. The resolution of a single pixel is therefore 0.22". The observations were carried out in four bands ($g\acute{}$, $r\acute{}$, $i\acute{}$, $z\acute{}$) in the Sloan Digital Sky Survey *u'g'r'i'z'* magnitude system. Most observations were performed in the *r'*-band, however, all other bands were also observed regularly during the night, between the *r'*-band observations. This technique allows for a better asteroid colour determination scheme as well as distinguishing colour variation for phased photometry than by using a single filter each night.

The asteroid (39420) 2084 T-2 was observed during 7 nights. Due to large uncertainties in the standard star observations during the first night, that was decided to be discarded. Therefore, the data used was from six nights between 21st and 29th September 2009.

The second set of follow-up observations occurred between the 11th and 14th December 2009 with initial data reduction performed by J. Pittichova in the V and R bands of the Johnson-Morgan $UBVRI$ magnitude system (hereafter FU 2 observations). These observations were also taken with the University of Hawaii 2.2-m telescope.

Furthermore, relevant data from the Lowell observatory database (Oszkiewicz et al. 2011) was added to the used data set. The criterion used to hand-pick data from the Lowell observatory database was its abundance during a single apparition. This would provide a sufficient coverage of observational geometries throughout the large variety of angles. A sample of data from four different apparitions was chosen, comprising observations from 44 nights.

3.2 Photometric data reduction

The images were taken in the FITS format, a *de facto*-standard for photometric images. Each image comprised a 2048 x 2048 matrix, including an overscan area for automatic dark current reduction, and a file header with metadata of observations.

Initial data reduction consisted of calibrating images with bias and flat-field corrections using the IRAF software (Tody 1993) with the SAOImage DS9 software (Joye & Mandel 2003) as a visualization application. First, the reduction of images was conducted using the *noao/imred/ccdred* package with the routines *zerocombine*, *flatcombine* and *ccdproc*. The images have not undergone a dark current correction provided by the instrument, but since the dark current is very small, the effect on the observational error is negligible. The magnitude of the asteroid from different images is calculated by comparing it to the magnitude of the observed standard star with a defined constant magnitude at each of the four used filters.

During each night, a set of several standard stars at different air mass values were observed. The used standard stars are all extracted from the $u´g´r´i´z´$-standard star catalogue (Smith et al. 2002).

The magnitudes of the asteroid and different standard stars is measured using the *phot*-function in the *noao/daophot/digiphot* package. The instrumental photometry was compared and reduced using the photometry of standard stars taken at different air mass values every night. The standard star images were separate from the asteroid images, so the method used was relative photometry.

The airmass function is expected to conduct a linear behaviour as the zenith angle of observations does not exceed 60°. The airmass coefficient k is therefore a linear least-squares fit of airmass – magnitude difference points (Nilsson et al. 2006) at each filter:

$$m - m_0 = kX,$$

where m and m_0 are the observed and catalogue values of the standard star magnitudes and X is the airmass.

The airmass and observational epoch were extracted from the FITS header by a combined IRAF/Python script and the function of airmass and difference of magnitudes was interpolated throughout the possible airmass value space. Some standard stars were overexposed during observations and were therefore omitted from the fit. The real visual magnitudes of asteroids were obtained by subtracting the difference between the observed and catalogued magnitude of a standard star at the air mass value of the asteroid at the corresponding filter.

The visual magnitude was further reduced to the reduced magnitude $H(\alpha)$ (Dymock 2007)

$$H(\alpha) = V - 5\lg(r\Delta),$$

where V is the visual magnitude and r and Δ are the asteroid's distances from the Sun and the Earth respectively.

The asteroid was initially tracked from the FITS image by using the ephemeris from JPL's online HORIZONS ephemeris service (Giorgini et al. 1996). The service was also used to calculate geocentric and heliocentric Cartesian coordinates at each observation epoch. These coordinates were used to calculate the topocentric and heliocentric distances of the asteroid as well as during the scanning of the rotational period of the asteroid.

The data was also light-time corrected, i.e. the time during which the light traveled from the asteroid to the observer has been subtracted from the observation time. While this difference is small, it is substantial in period determination, as small mutual inconsistencies sum up.

A Python program was written for indexing the data, implementing a linear least squares fit for standard stars at different air masses, calibrating the asteroid

data according to the results of the standard star fit and plotting the results at different bands.

3.3 Lightcurve inversion software

This section presents the used mathematical and scattering models as well as the flowchart of the lightcurve inversion software used (Kaasalainen & Torppa 2001, Kaasalainen et al. 2001, Ďurech et al. 2009) which consists of three separate parts.

The derivation of information about an asteroid from its lightcurve is an inverse problem which entails solving for the asteroid's rotational period, shape and orientation in space.

The period is calculated using a robust shape with six initial rotational pole guesses. The final result is a convex polyhedron with triangular facets, representing a convex model of the asteroid. In particular, the model does not reproduce the possible concavities, such as valleys or craters, but rather hides all such shape information beneath the convex cover. Therefore even close binaries are modeled as single, albeit elongated objects with large smooth surface facets covering concave areas. Differences between the fit and the observations, such as a more smooth fit curve can however reveal concavities and binary properties (Ďurech & Kaasalainen 2003).

The convex inversion software assumes a combination of Lambert and Lommel-Seeliger scattering laws as a physical model. The Lommel-Seeliger law represents single scattering whereas the Lambert law represents multiple scattering. The terms are combined by assigning weight coefficients to thhe scattering law functions and multiplying them with a function of the phase angle:

$$S(\mu, \mu_0, \alpha) = f(\alpha)(S_{LS}(\mu, \mu_0) + cS_L(\mu, \mu_0))$$

$$= f(\alpha)\mu\mu_0(\frac{1}{\mu+\mu_0} + c),$$

where

$$f(\alpha) = ae^{-\alpha/d} + k\alpha + 1,$$

and where μ and μ_0 are cosines of the reflecting and incident angles of light respectively, α is the phase angle, a and d are amplitude and scale length of the opposition effect, k is the coefficient of the decreasing phase curve slope, and c is a weight factor. Although the presented model is rather simple, it nevertheless produces results similar to more sophisticated scattering models such as the Lumme-Bowell law (Kaasalainen et al. 2002). The advantage of using this model is its computational efficiency while the major limitation of the model is its inability to reproduce shadowing (Wilkman & Muinonen 2013). The opposition effect is however mimicked with the exponential-linear phase function.

The first step is performed using the period scanning software (*period_scan*). The period scan is performed by using an ellipsoid as an initial model for a period fit with six random pole orientations. The best fit (in the sense of minimum root mean square (rms) deviation) is then chosen. The vicinity of the local minimum is further scanned with a smaller interval to obtain the true local minimum.

The second and main part of the lightcurve inversion is performed using the *convexinv* program. The program takes the period, angle coordinates of the pole orientation, as well as the shape of asteroid and varies them in order to iteratively solve the best fit which is once again defined by the smallest rms deviation value. Even if a period is known reasonably well, several runs with different initial pole values are nevertheless required because local minima to which the iterations converge are rather strong. The parameters describing the scattering law, resolution of vertices as well as convexity regularisation can all be adjusted in the parameter file.

The package also includes two programs which produce the output suitable for visualizing the resulting shape. The first one (*minkowski*) solves the coordinates and vertices of surface simple polygons as well as their mutual connections while the second one (*standardtri*) converts these polygons into triangles.

In case the period and pole orientation of the asteroid are known with great precision, they can be fixed and the shape can then be optimised with the *conjgradinv* software.

A third separate part is a synthetic lightcurve generator (*lcgenerator*) which produces lightcurves at given epochs and geometries. The program uses the shape model, the period and the orientation of the asteroid as input values. It is used to visualize the lightcurve which the model solved by the *convexinv* software and compare it to observations. The model which produces the best fit for observations is then picked as the final solution.

The software is maintained along with the DAMIT database (Ďurech et al. 2010) which includes convex shape models for asteroids. Currently (2013) there are shape models for 347 asteroids stored in the DAMIT database.

3.4 Period fitting

The period determination in this work was carried out by using the *period_scan* software. The bulk of the data for the lightcurve inversion is the data from TALCS and FU 1 observations. The majority of FU 1 observations was conducted in the *r'*-band. Other bands were decided to be excluded in the lightcurve inversion process as the shapes of lightcurves are the same in all bands. No additional information required for period determination is therefore included in other bands. Moreover, the possible uncertainties from the colour shift could have introduced unnecessary errors.

The period search was performed using the *period_scan* software. The Fourier

analysis of Harris et al. (1989) which is a common tool in period determination was not used because it was deemed not suitable for a long period asteroid with sparse data.

Various combinations of data sets were attempted to use in order to obtain the period. The final data set for period scanning consisted of FU 1 observations as a single lightcurve, FU 2 observations as a separate single lightcurve and TALCS observations converted to a single filter as the third separate lightcurve. The Lowell data was left out from the final period scan because it proved to increase the overall level of the rms deviation values and did not contribute to the fit. It must be noted, however, that preliminary attempts including the Lowell data pointed out some reasonably good period candidates.

The input for the *period_scan* software includes, the observational epoch, relative magnitudes and heliocentric and topocentric Cartesian coordinates. The zero-level for relative intensities is chosen for each observation set and is further adjusted by the software. The local rms deviation minima are chosen as solution candidates.

The period scanning was carried out using relative intensities between observational data sets but absolute within a single data set. The reference level was scaled to be the average magnitude level at each apparition. It must be noted that the magnitudes in question were the above-mentioned reduced magnitudes, as the phase function is resolved by the software.

The guideline definition for a unique period solution by the period scanning software is that the rms deviation value of the fit is ca. 10% lower than all surrounding values (Ďurech et al. 2009). Since no such solutions exist, several local solutions are examined thoroughly.

The preliminary result for the period obtained in TALCS was 105 h ± 21 h. First, a general scan on the entire period area from 0.1 to 130 hours was performed. The time step used varied slightly, but was always around 0.01 hours. The second

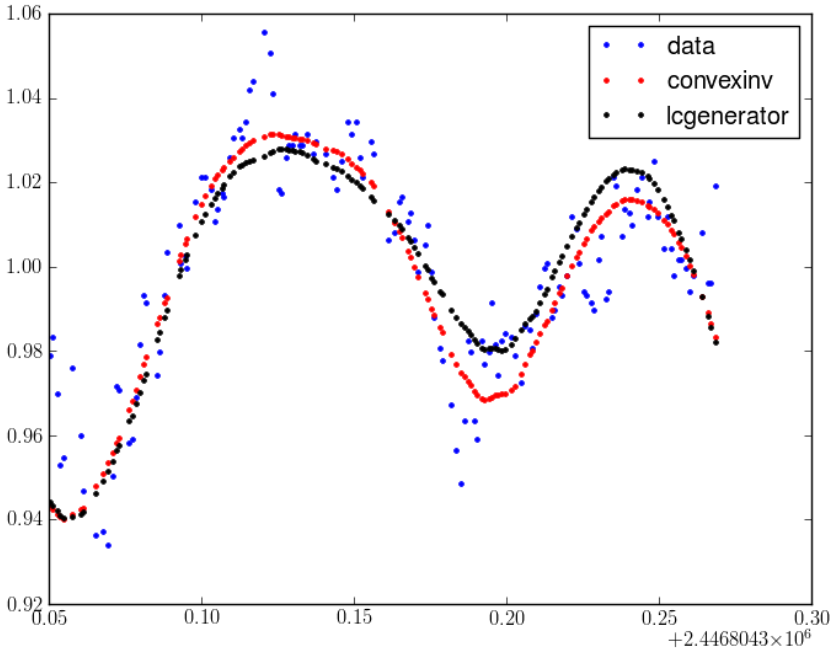

Figure 3.1: The extract of the data, convex lightcurve inversion fit and a synthetic lightcurve of the asteroid (43) Ariadne.

phase contained a more thorough period scan with an average time step of 0.0001 hours on the period fit rms deviation local minimum areas in order to determine the real local minima.

In order to confirm the correctness of the used method, a separate assessment working example of the *convexinv* software has been made. The data used for this example was the lightcurve of asteroid (43) Ariadne provided together with the software. The results obtained from this working example were in accordance with the results published in the DAMIT database, rendering that the method was used correctly in the case of the present work. The extract from the fit for the asteroid (43) Ariadne is presented in Fig. 3.1.

3.5 Convex shape inversion and pole solution

The solution of the shape of an asteroid is closely tied to its orientation in space. The input values of the *convexinv* software include the photometric observations, the ecliptic latitude and longitude of the rotation pole of the asteroid and the rotational period, in addition to mathematical and physical parameters required to define the scattering model and determination of the convex shape model. The pole orientation and period are then iterated in order to obtain an optimal model.

Conventionally, one lightcurve corresponds to observations obtained during a single night which are consequently adjusted to a single level between nights. This primary method is created to meet the common situation of asteroid observations being only relative, i.e. not calibrated to absolute magnitudes with standard star observations. This method is usually sufficient enough for short-period asteroids which comprise the majority of asteroids with shape models because the entire range of phase angles or at least a significant part can be covered during single night observations.

The discussed method is, however, not suitable for the current situation because magnitude variations between nights are significant and the phase is not covered during a single span of observations. The solutions for this set of observations is either to treat them as a single lightcurve or convert them to absolute values. In this case, observations comprising a single data set from different nights were combined into a single lightcurve.

It should be noted that the differences in observational geometry of irregularly shaped bodies (which small asteroids usually are) result in lightcurves that look completely different compared to each other.

The unique solution of the rotation longitude could be obtained if the rms deviation value minimum would appear to be significantly smaller than other candidates in the random search for pole direction. Unfortunately, it was not the case, as

there were several solution candidates. Additionally, the fit of the noisy data from the Lowell Observatory database gives a value span of $29.8° \pm 49.0°$ for the rotation axis longitude (Bowell et al. 2013). This is a rather broad span of possible solutions, and in this case, one must resort on secondary means to narrow the solution candidate space.

The prominent feature of the lightcurve is its exceptionally high amplitude. This indicates that the rotation-axis vector is close to being perpendicular to the topocentric vector. By using the values given by this perpendicular vector as an initial guess for the rotation-axis longitude and latitude, one can search for a local minimum in the vicinity of these solutions using the *convexinv* software.

The situation is visualized in Fig. 3.2. The plane containing the pole vector in question is constructed by projecting the topocentric longitude on the abscissa (pointing to the vernal equinox).

The three components of the above mentioned pole vector are computed from the scalar product of the pole vector with the topocentric vector as well as its projection to the ordinate (perpendicular to the vernal equinox). The third degree of freedom is constrained by solving the normal vector to the plane restricted by the topocentric vector and its longitude projection on the abscissa. The longitude and latitude angles are then calculated from scalar products of the vector with the axial unit vectors.

Topocentric and heliocentric longitudes for observations were calculated using the OpenOrb software (Granvik et al. 2009). The epoch during which the pole was calculated was the one among the FU 1 observations as these observations showed the highest amplitude among different available observation sets. The solution for the pole orientation perpendicular to the topocentric vector was for longitude $\lambda = 117.7°$ and for latitude $\beta = 15.4°$.

Because the initial guesses of the pole orientation were contradictory, it was

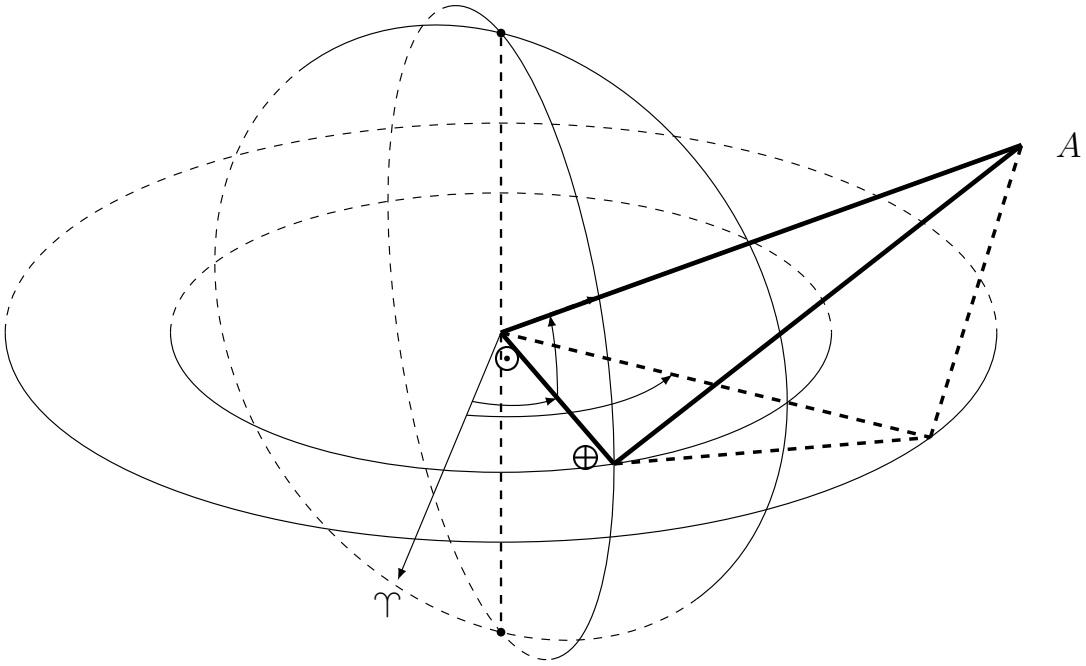

Figure 3.2: A scheme representing the geometry of the Sun, the Earth and the asteroid (A). The rotation axis of the asteroid is assumed to be perpendicular to the topocentric vector.

decided to perform the convex inversion through the entire latitude-longitude space with a 10° resolution to reveal the global minimum rms deviation fit. The synthetic lightcurve using the *lcgenerator* program is then produced using local minimum solutions. The generated lightcurves are then visually inspected to empirically determine the best fit to observations.

3.6 Phasing data and residuals of the fit

The phasing of data entails arranging all observed data by using a rotational phase of the asteroid on the abscissa instead of observation time. Data arranged in that way reveals at a glance if the period solution is physically plausible.

The zero point for phasing is arbitrary. Since observations were able to cover a single rotation maximum of the asteroid it is natural to choose this maximum point

as the zero point.

The residuals are obtained by using the output lightcurve computed by the *convexinv* software. The file gives values of the relative intensity of the fitted lightcurve at the same observation epochs as observations. The residuals are then computed by simply subtracting the points produced by the fit from the observations.

In order to become a solution candidate, the calculated period should satisfy several conditions. First, it should be a local minimum of the period fit rms deviation. Second, the phased lightcurves of the same observation set (i.e. multiple-night lightcurve) may not overlap in a contradictory way, i.e., having large magnitude differences or different slopes. Third, the residual values of observations and fit should be contained within the observational error of each given observational set and show a random error (and specifically not systematic error) behaviour.

The phasing of the data was performed on selected local and the global period scan rms deviation minima. A small rms deviation value indicates that the fit is good numerically, but does not provide information on whether the solution is physically possible or not. The separate examination of data phasing in combination with examining residuals of the lightcurve fit provide a means to deduct if the possible solution is physical.

The solution for the period of (39420) 2084 T-2 from (Masiero et al. 2009) was 105 ± 21 h. The search for a possible period solution was therefore concentrated in that area. However, in order to verify the results, the period scan was conducted for solutions from 0.1 to 190 hours.

4. Results

4.1 Reduced photometry

For this study, the photometric reduction has been conducted for FU 1 and partially FU 2 observations (bias and flat-field reductions have been previously conducted for FU 2 observations).

The results of photometric reduction of FU 1 observations confirmed the exceptionally high amplitude and slow rotation rate of asteroid (39420) 2084 T-2.

The colours obtained from the images are presented in Table 4.1. The $g´$-$r´$ values of Masiero et al. (2009) have been improved due to the observational cadence used which is more suitable for slow rotators. The colour value from the TALCS and FU1 observations are contradictory, being 1.913 ± 0.050 from TALCS and 0.515 ± 0.026 from the FU1 observations. The colour index calculated from the FU 1 data was decided to be used. The FU 1 data includes observations in all bands from every night whereas TALCS performed exclusively $r´$-band observations on a single night and exclusively $g´$-band observations otherwise.

The brightest values of observations (i.e. lowest magnitude values) are obtained in the red r' band. No high precision spectroscopy has been performed, and the results in four filters are only approximate. However, the exceptionally high geometric albedo of 0.5 ± 0.1 would point the asteroid (39420) 2084 T-2 to belong to the E-type according to the Tholen taxonomy (Tholen & Barucci 1989). The E-type

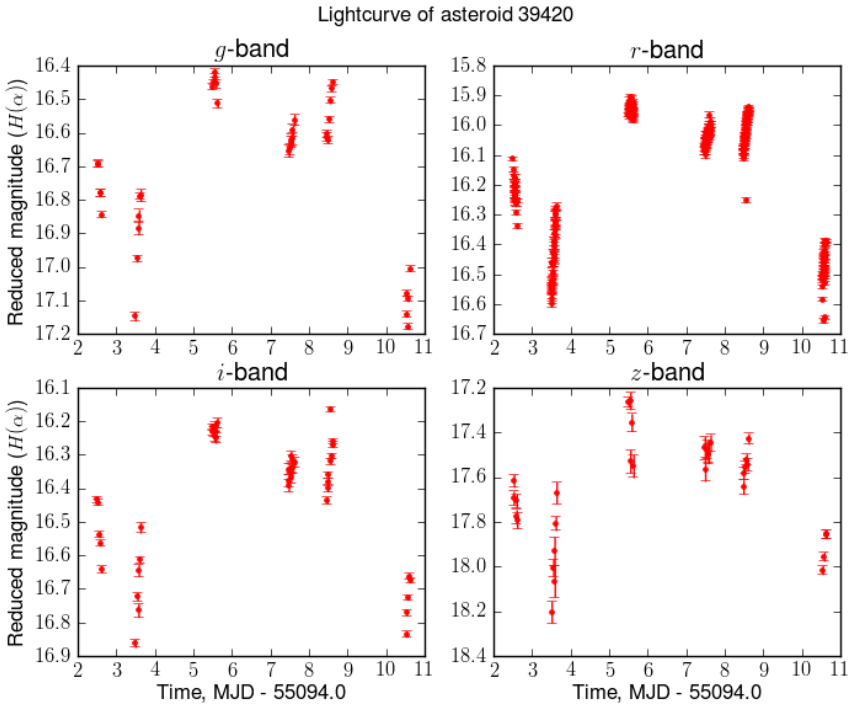

Figure 4.1: The results of observations in 4 bands.

Colour	Value	Error
g' - r'	0.515	0.026
r' - i'	-0.273	0.020
r' - z'	-1.500	0.100

Table 4.1: Defined colours.

is common among Hungaria asteroids and rare in other asteroid populations. The obtained colour values do not contradict this theory.

The resulted data in four observed bands ($g\acute{}$, $r\acute{}$, $i\acute{}$, $z\acute{}$) are presented in Fig. 4.1.

The prominent features of the FU 1 observations are long increasing or decreasing slopes as well as a very sharp maximum. These features along with the long rotation period point to the asteroid being either very elongated, a binary, or in a non-principal-axis rotating state.

No significant variation in different photometric bands has been observed which means that in the case of asteroid being a binary, the components have the same origin.

4.2 Lightcurve period and shape inversion

The aim of the convex inversion is always to find a unique combined period, shape and pole orientation solution for the used data. The goal is commonly met for asteroids with short periods (see e.g. data in Ďurech et al. 2010). However, the limitations of the current data, most notably its inability to cover the entire phase continuously, do not permit an unambiguous solution.

Based on solely the period determination scanning, one cannot unambiguously determine the period of the asteroid because there are several local rms value minima (see Fig. 4.2). Using only the period scan, it is not possible to establish whether the asteroid (39420) 2084 T-2 is a slow rotator because there are several local minima throughout the scan interval. The phasing of data permitted to exclude all potential period solutions beneath 60 hours. Of all of these solution candidates, there was at least one inconsistency of overlapping lightcurves from the same apparition. These inconsistencies were large magnitude differences that, on the one hand, cannot be explained by observational errors or shifts of phase angles, and on the other hand, contradicted or even had opposite-direction slopes of lightcurves compared to similar data from the same observation set.

The minimum rms value occurs around a period of 78 hours. Thus, the convex shape inversion has been concentrated in that area. The entire latitude-longitude space was studied systematically to find an optimal solution (see Fig. 4.4). As one can see from the figure, the best results, apart from a single point, are situated in the same area. This area falls within the longitude obtained from Lowell database (Oszkiewicz et al. 2011) which was $29.8° \pm 49.0°$. The rotational pole of the asteroid

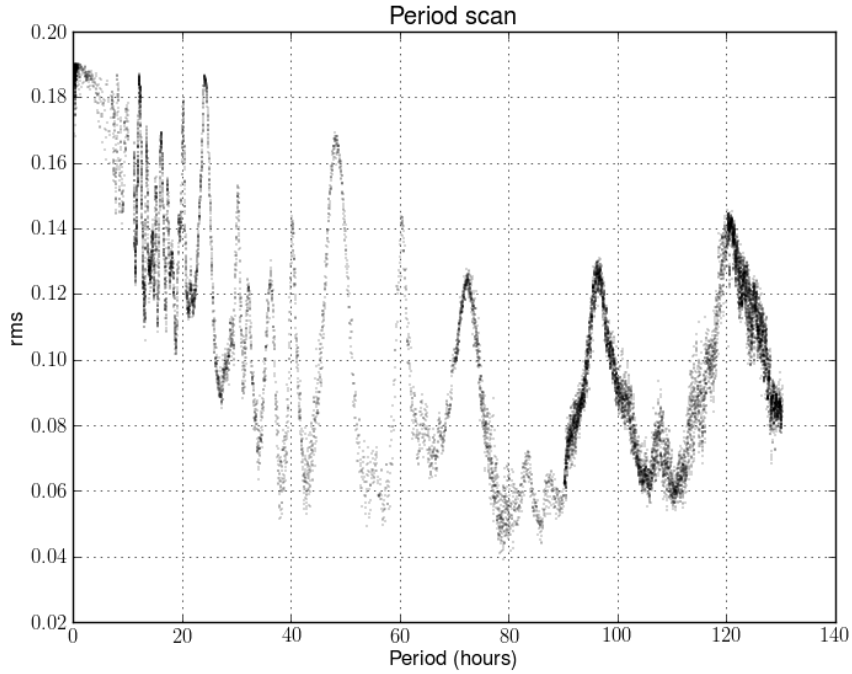

Figure 4.2: The period scan from 0.1 to 130 h with an approximate step of 0.01 h as a function of the root mean square value of the fit. The minimum is near 78 h.

is, however, not close to perpendicular to the topocentric vector, as was anticipated in section 3.5.

In addition, a pole search was performed at a local root mean square deviation minimum near 156 hours (Fig. 4.3) for reference purposes.

The comparison of observed data and modeled data is presented in Fig. 4.5 and the residuals of that fit is presented in Fig. 4.6.

All convex shape inversion fits were not far from each other in terms of the values of the rms deviation but the actual goodness of these fits varied significantly. The common property for all fits was the elongated shape of the convex model. No model was good enough to fit well into all different sets of observations. The presented result was chosen because it was the best fit for the FU 1 observations and because these observations comprise the main bulk of all data. The fits to different data sets are presented in Fig:s 4.7, 4.8 and 4.9.

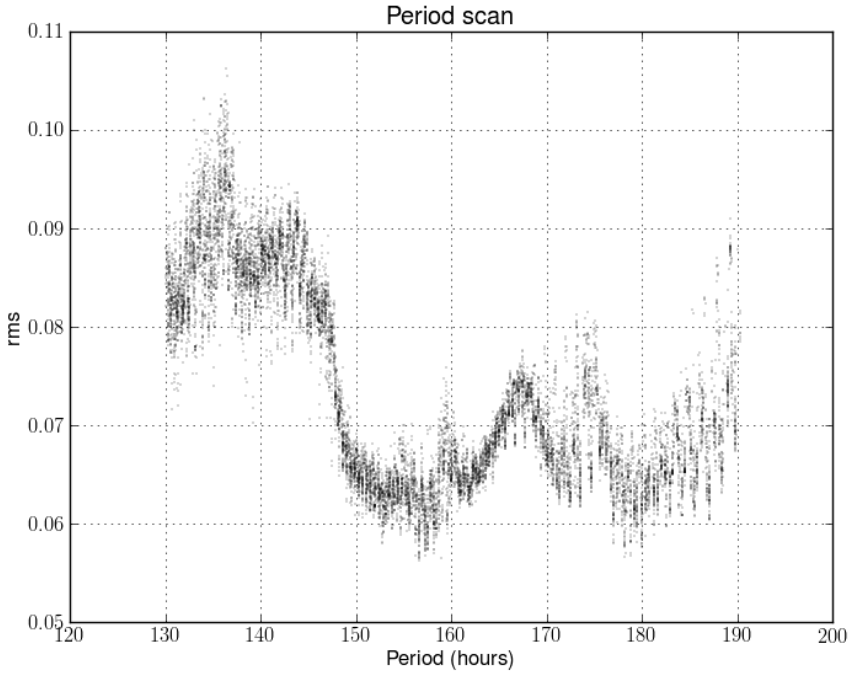

Figure 4.3: The period scan from 130 h to 190 h with an approximate step of 0.01 h as a function of root mean square. The local minimum is near 156 h.

The periods found are able to reproduce the FU 1 observations but neither the sets of TALCS observations nor the FU 2 observations. In fact, separate fits with different periods would work better. This would imply that the asteroid does not have a single well-defined rotation state and is therefore a non-principal-axis rotator.

Not a single fit was able to reproduce the steep nature of the maximum turn. This situation is the same as discussed by Ďurech & Kaasalainen (2003) where the lightcurves of convex models are smoother in shape than the steep maxima and minima of concave objects and binaries. Based on this feature of the lightcurve, it can be claimed that the asteroid (39420) 2084 T-2 could be a binary or a contact binary and not a smooth elongated body such as e.g. the recently extensively observed (25143) Itokawa.

Empirically the best and, thus, presented result for the period, shape and pole

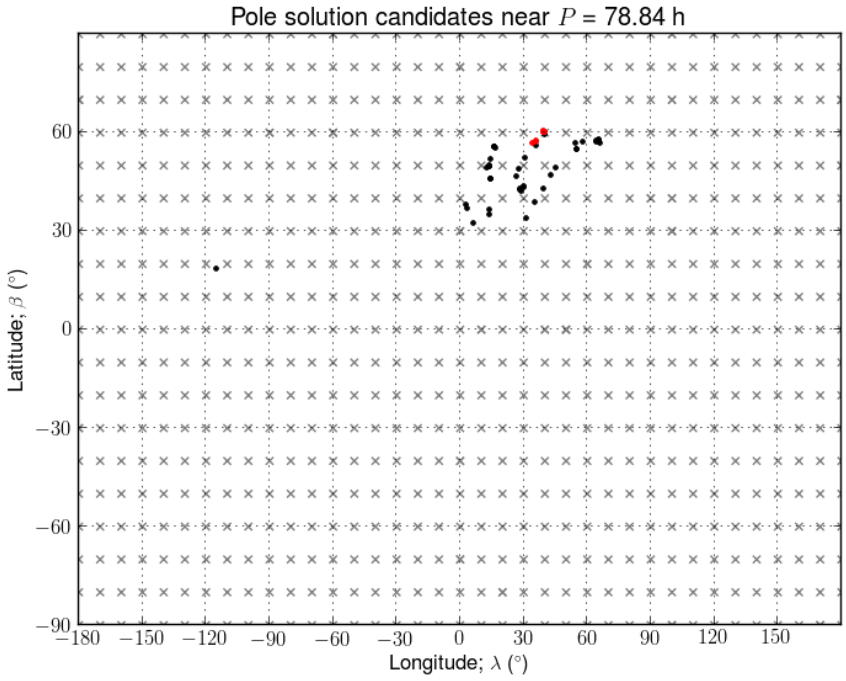

Figure 4.4: The pole solutions near 78.84 h. The grey crosses are the attempted input values of pole solutions. Black points represent the solutions with 0.037 < rms deviation < 0.039 and red points represent output solutions with rms deviation < 0.037 (best solutions).

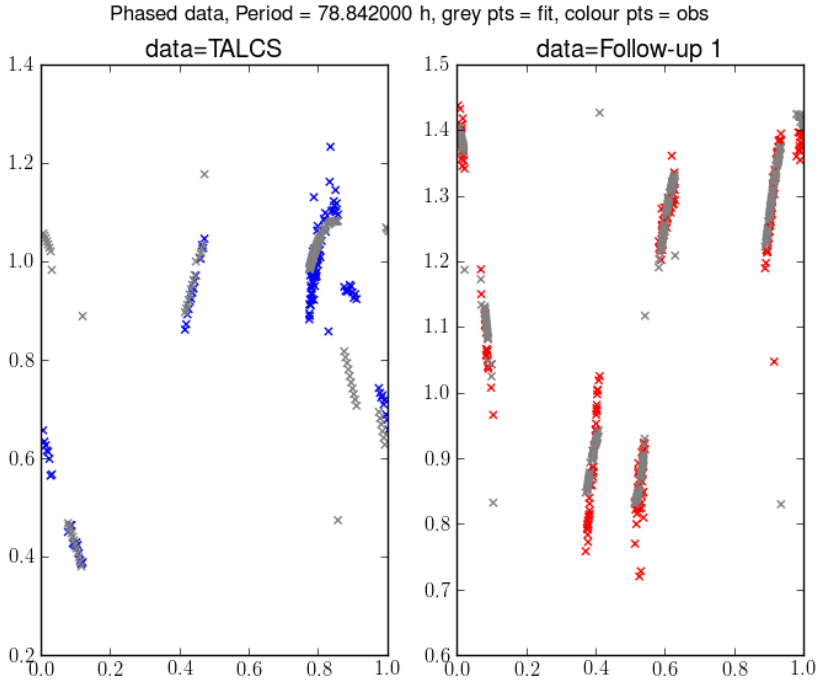

Figure 4.5: The phased data and convex inversion model fit for the period of 78.84 h.

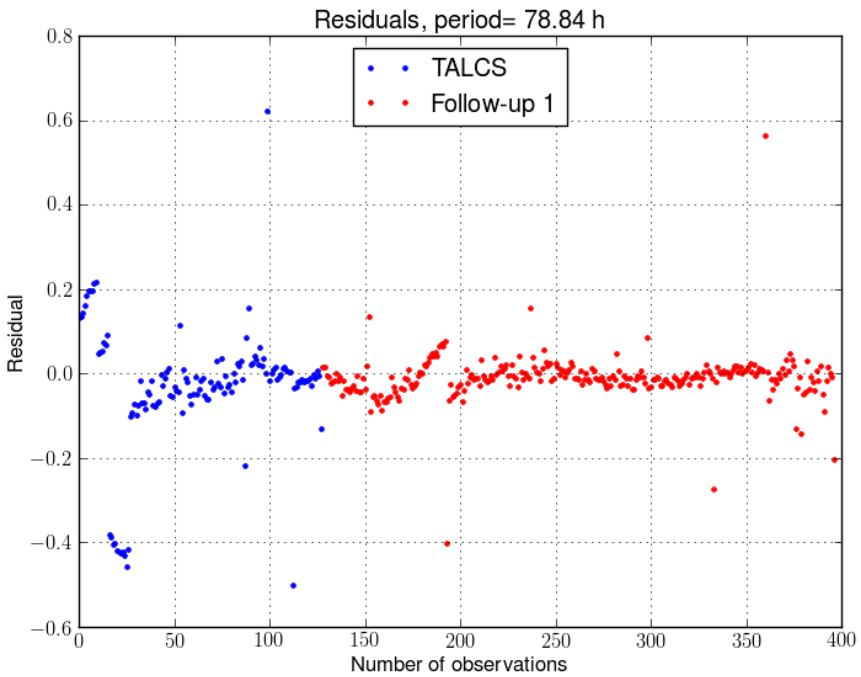

Figure 4.6: The residuals of the fit for the period of 78.84 h.

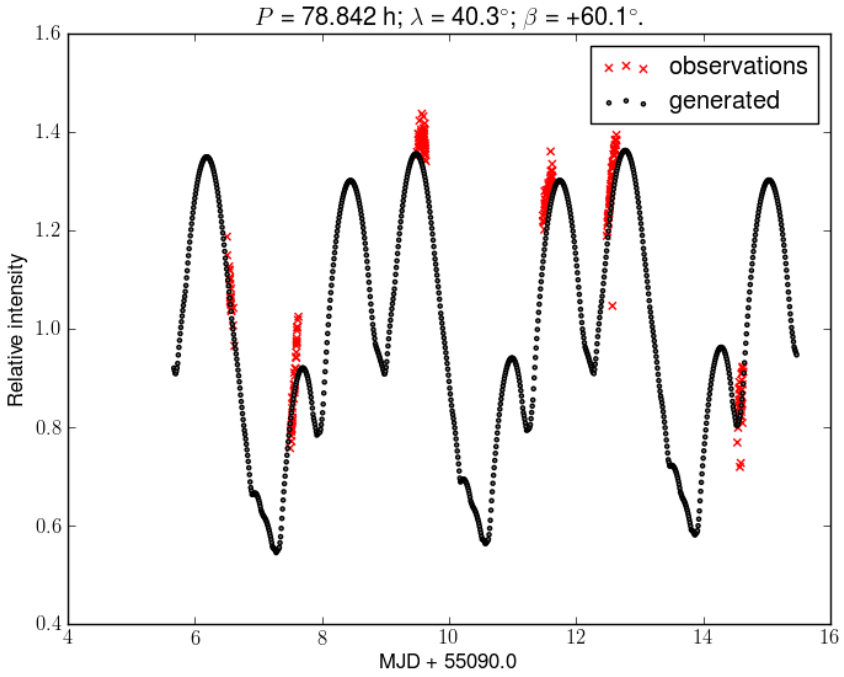

Figure 4.7: The best synthetic lightcurve fitted into FU 1 observations.

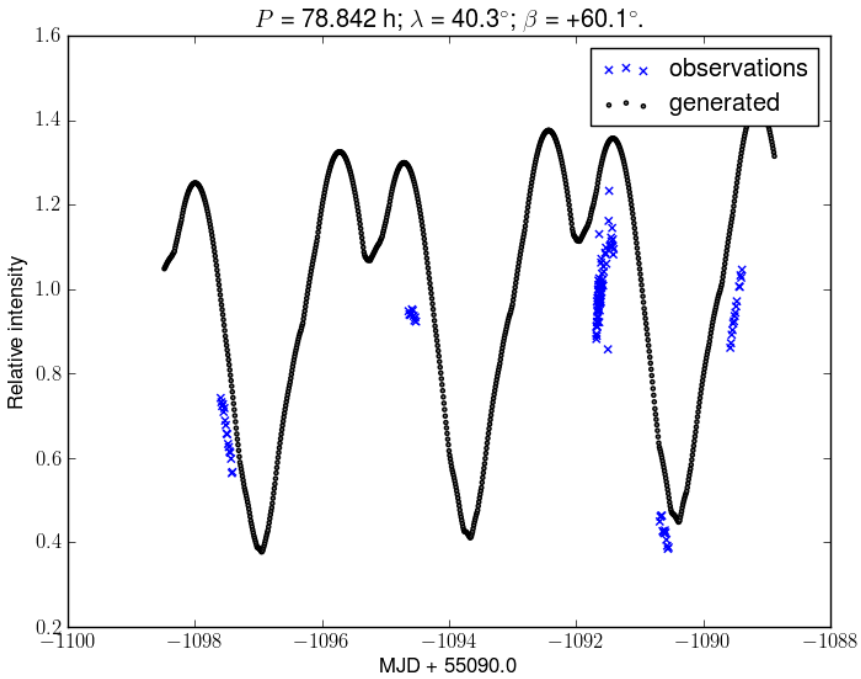

Figure 4.8: The best synthetic lightcurve fitted into TALCS observations.

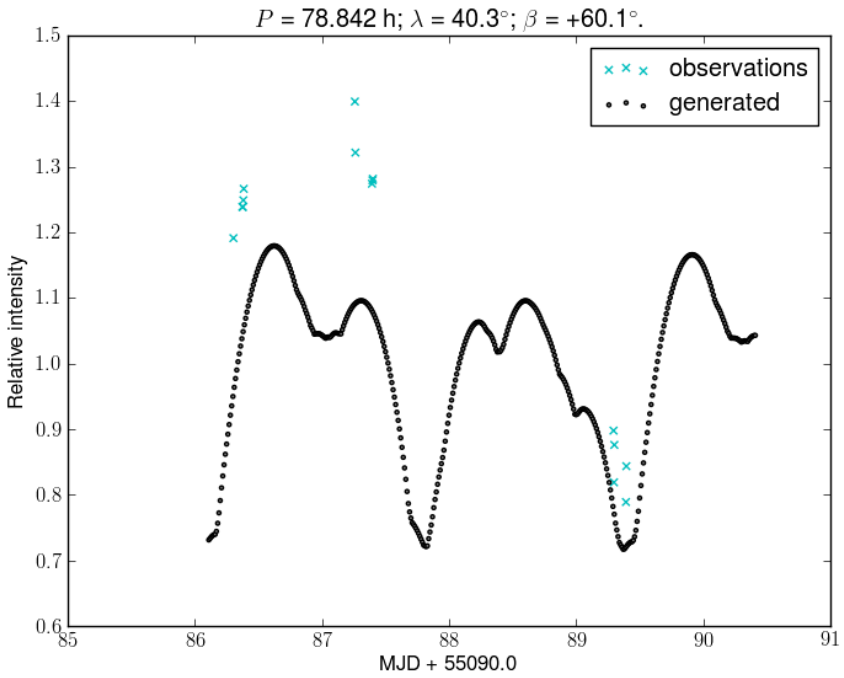

Figure 4.9: The best synthetic lightcurve fitted into FU 2 observations.

solutions are: rotational period $P = 78.84$ h; rotation longitude $\lambda = 40.3°$; rotation latitude $\beta = 60.1°$.

The best convex shape model of the asteroid is presented in Fig. 4.10. The figure is produced using Matlab's *fill3* routine.

The location of the asteroid (39420) 2084 T-2 in rotation period-size phase space is shown in Fig. 4.11.

The general applicability of the convex model was shown in subsection 3.5. However, since the model fit was not satisfactory, it needs to be confirmed that the approach used in this work is suited for the specific problem, i.e. a slow rotator with a high amplitude of magnitudes. For this purpose, a synthetic lightcurve using the convex shape model of the elongated asteroid (624) Hektor (stored in the DAMIT database) and a period of ca. 100 hours was created using the *lcgenerator* software. The epochs of the synthetic lightcurves corresponded to the epochs of TALCS and FU1 observations. Some random Gaussian noise was added to the data. Finally, a

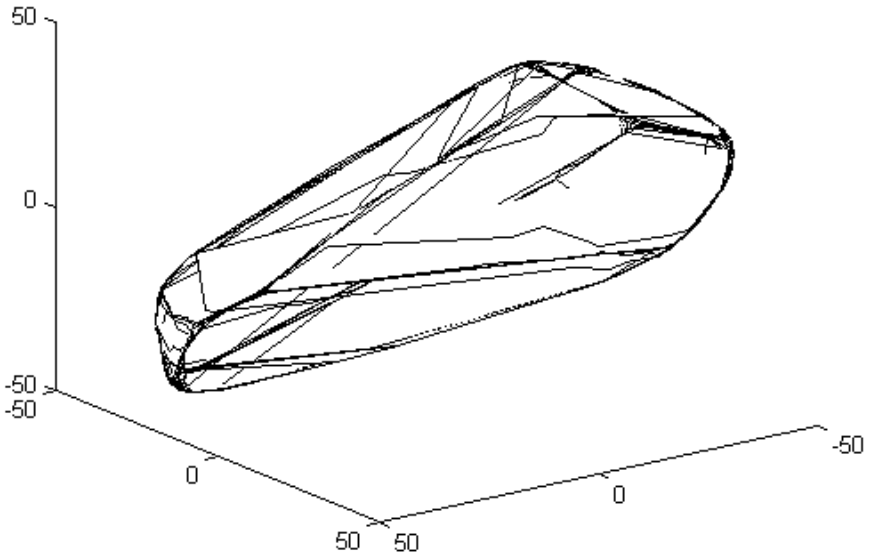

Figure 4.10: The two-dimensional projection of the three dimensional best convex model shape of the asteroid (39420) 2084 T-2.

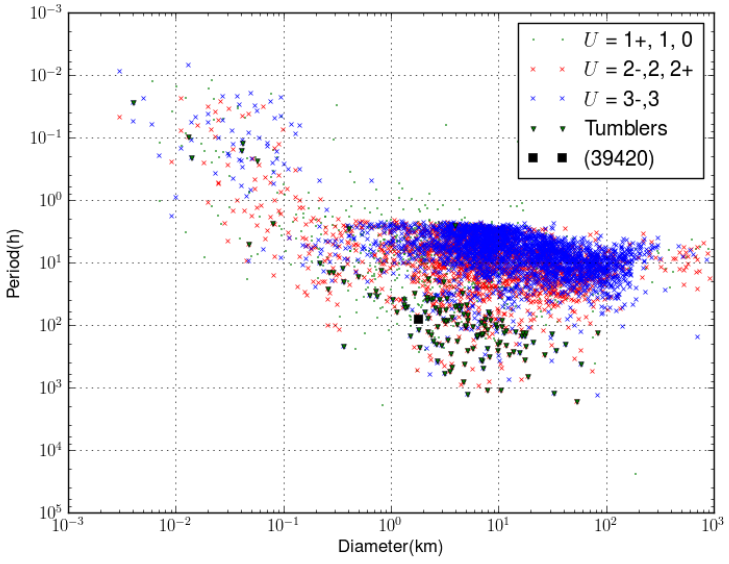

Figure 4.11: The rotation rate distribution of all asteroids with a known rotation period (even if it is poorly known, cf. to Fig. 1.2). The non-principal-axis rotators are marked with a green triangle and the asteroid (39420) 2084 T-2 is marked with a black square.

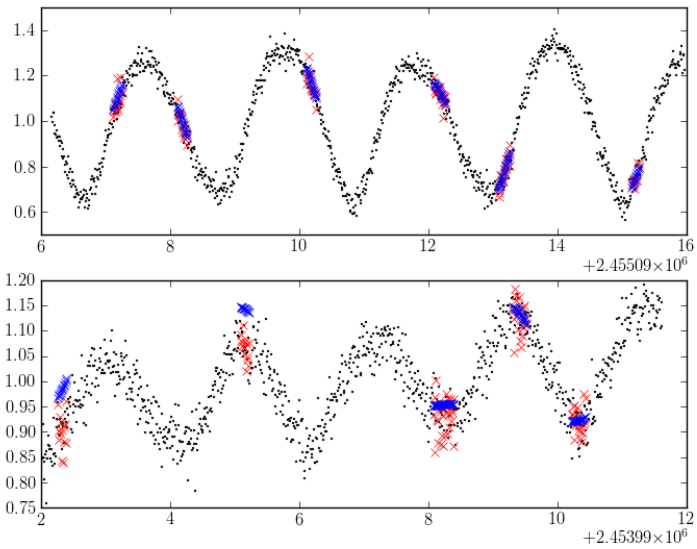

Figure 4.12: A test of applicability of the method to elongated objects with a long period. Black points represent the general trend of synthetic data. Red crosses are selected "observation" points selected for the convex inversion and blue crosses are the result of the convex inversion.

lightcurve shape inversion was performed using the *convexinv* software.

The problem with this approach is the possible inverse crime, (i.e. using the direct problem to derive the data to be used in the inverse problem, e.g., Wirgin 2004) induced by using the similar algorithms for creating the data and inverting it. Since this computation is used only for validation of the method, the problem is not so essential. Furthermore, the algorithms are separate, and in case the *convexinv* software produces dark facets in its solution, also the results are different. Therefore, the algorithms of *convexinv* and *lcgenerator* are slightly different. In addition, the data has been modified to further reduce the inverse crime issue.

The results of the test are presented in Fig. 4.12. As can be seen, fits are very good for one set of observations but not very good for the other observational set. Though the second fit is not very good, it is nevertheless completely within the error bars of observations.

The results of this test indicate, that the method is suitable for fitting lightcur-

ves of elongated slow rotators. Therefore, the problem of the inability to make a decent convex inversion lies within the assumptions of the model, which are that the body is single and in a principal-axis rotation state.

5. Discussion

The initial period scan attempts were performed using single lightcurves. These period scans were able to produce only wide local minima area with nearly the same root mean square deviation values. Therefore, the results were mutually indistinguishable. Though it was possible to find local minima with the help of additional data, one cannot be absolutely certain that the result is correct, because sparse data had large uncertainties.

The new facilities, such as Pan-STARRS, are able to provide quite accurate sparse photometric data regularly. The upcoming data from Pan-STARRS will also be absolute in addition to being accurate, further enhancing the quality of future lightcurve fits. Another asteroid lightcurve survey conducted with better data could be performed when there is a substantial amount of sparse accurate photometry available to test how well does it suit the purpose of lightcurve shape inversion.

The sparse data will not be adequate enough to ruling out the periods of slowly rotating asteroids. However, it will be suitable to enhancing period solutions for fast rotators (Ďurech et al. 2009).

One problem with the existing lightcurve inversion methods is that they do not take observational errors into consideration. While dedicated photometry usually has small errors, the sparse photometry does not, as it is usually a by-product of astrometric observations with short exposure times.

Though the goals of the TALCS and FU 1 observations were different it must

be noted on a general level that especially for slow rotators the "nested" observations of different filters remove colour unambiguity from the fit. In addition, observations from different nights with one observation set must be treated as a single lightcurve or all observations should be converted to absolute values. The latter is, however, not always possible to calibrate if the data set is compiled from various sources. The problem is that relative lightcurves do not contain enough information about brightness variations during a single rotational phase (especially for slow rotators) and are just adjusted to the same level with other observations, without any regards to their real photometric values.

Low-precision sparse data was decent for initial period scan but it was left out in the final stage of the fit. The high quality data from dedicated observations could probably be weighed by repeating in the construction of lightcurve in proportion to the difference of error bars of precise and non-precise data. The weighing mechanisms could also be directly implemented in the method.

The limitation of the model used is the assumption of an asteroid being a single convex object with a principal-axis rotation. Clearly, the poorness of the fit indicates that the limitations of the model are serious in this particular case. The very sharp turn in the the FU 1 observations at MJD 55099 could be an indirect indication of the asteroid (39420) 2084 T-2 being a binary, analogically to Ďurech & Kaasalainen (2003).

In the case of sparse data, finding the global minimum of a convex shape inversion is not trivial because there are so many gaps where no information on the data exist. This is a major problem especially for slow rotators. In case of applying alternative approaches for solving the inverse problem, namely Bayesian methods which can sample the entire solution space, such as Markov chain Monte Carlo methods, the problem still remains.

The TALCS observations of asteroid (39420) 2084 T-2 suggested a rotation

period of 105 ± 21 h. The result obtained by adding the FU 1 observations, i.e. 78.84 h, lies slightly outside the error bars. Other slow rotators observed in TALCS also have large error bars. Therefore, one could argue that the error bars presented in TALCS should be even larger. Based on a single lightcurve (which in the case of slow rotators can span several nights) it is not always possible to postulate whether the slowly rotating asteroid is in a principal-axis rotating state or not. Therefore, the possible explanation for large error bars could be that the asteroid is a non-principal-axis rotator.

The hypothesis of the asteroid (39420) 2084 T-2 being in a non-principal-axis state is further enhanced by the fact that among the slowest asteroids with similar properties ($D \approx 2$ km, $A \approx 1.0^m$), i.e. (3288) Seleucus, (4179) Toutatis and 1999 JM8 are all in fact tumblers (Harris 2002). The found period 78.84 h is a global minimum of the rms deviation for the period scan, so it can be picked as the main candidate for the main rotation period P_ψ (see section 2.1) of a non-principal-axis rotator. The inability to obtain a unique period solution has been a valid argument in declaring the asteroids to be in a non-principal-axis rotation state.

Harris (1994) defined the timescale of damping into the lowest energy state of principal-axis rotation by making certain assumptions about the structural and shape parameters of asteroids:

$$\tau = \frac{P^3}{C^3 D^2},$$

where τ is the damping timescale in 10^9 years, P is the rotational period in hours and D is the diameter of an asteroid in kilometres, and C is a constant containing the assumptions about the parameters of the asteroid. The value of C is not well known, but is estimated to be between 7 and 40. By inserting the values $P = 78.84$ h and $D = 1.8$ km for asteroid (39420) 2084 T-2, the lowest value of $\tau = 2.36 \cdot 10^9$ years is obtained. This timescale is around half the age of the Solar System. Pravec

et al. (2005) argued that the majority of asteroids with the damping scale beyond the age of the Solar System are non-principal-axis rotators. As can be seen from Fig. 4.11 the asteroid (39420) 2084 T-2 is in a location where tumbling asteroids appear in high numbers.

6. Conclusions

The performed study of the lightcurve of asteroid (39420) 2084 T-2 did not lead to any solid results on revealing the period, convex shape model and pole orientation. The study utilized photometric observations from 14 nights over the period of 2005 - 2009.

The steep maximum observed on MJD 54099 (see Fig. 4.1) is an indirect indication of the binary or contact binary features of the asteroid (39420) 2084 T-2. Any attempted convex model could not represent this feature. The other indication of a binary asteroid is a lightcurve clearly comprising two separate contributing components. The current data is not sufficient to verify or discard that possibility.

The inability to obtain a unique period solution is an indication of the asteroid being in a non-principal-axis rotation state. Separate assessments of the TALCS and FU 1 observations gave different results for the best period, which further supports the hypothesis.

The asteroid (39420) 2084 T-2 turned out to be a particularly interesting object. Unfortunately, the amount of existing data does not permit to obtain precise results. Therefore, more observations are required to reveal the true nature of this asteroid. Particularly observations from large phase angles can reveal possible concavities and reveal whether the asteroid is binary or a contact binary (Ďurech & Kaasalainen 2003). The largest maximum value of the phase angle available for observations is ca. 33°.

Summarizing the conclusions based on the analysis performed on the available data suggests that the asteroid (39420) 2084 T-2 could be a binary, a contact binary asteroid or in a non-principal-axis rotation state. The more likely possibility is an asteroid with non-principal-axis rotation. The steep turn at MJD 55099 supports the hypothesis of a binary asteroid but all other features (steep, long slopes of observations; long period and relaxation timescale far over the age of the Solar System; comparison with similar lightcurves of observed tumblers) are in support of the hypothesis that the asteroid (39420) 2084 T-2 is a non-principal-axis rotator. In fact, the majority of asteroids the damping timescale of which is of the same scale with the age of the Solar System are non-principal-axis rotators (Pravec et al. 2005). Comprehensive models suitable for solving the binary nature or the non-principal-axis rotation of an arbitrary are yet to be developed though certain single asteroids of both categories have been given appropriate treatment.

The results of this work could be used as a working hypothesis for further investigation of the properties of the asteroid (39420) 2084 T-2 and other similar objects from the TALCS (Masiero et al. 2009) and other observations. Also the verification and narrowing error bars of periods of slowly rotating asteroids (including observations by Masiero et al. (2009)) require more observations. It is important to obtain these results in order to debias the rotation rate distribution at the slow rotation end.

The interesting problem pending further investigation would be to address the questions, why some slow rotators exceeding the damping time scale of asteroids retain their principal-axis rotation and some do not. For example, could the outcome depend on the shape characteristics? In addition, applying the analysis performed in this work to other slow rotators with large error bars discovered in (Masiero et al. 2009) and other lightcurve surveys should be performed in the future.

It would also be interesting to assess the taxonomy of non-principal-axis ro-

tators, particularly in the Hungaria region. In an isolated population such as the Hungaria region, the close encounters with planets cannot decline the asteroids into the tumbling state. In an isolated population, the presumable mechanisms for non-principal-axis rotation are on one hand cometary activity and on the other hand YORP forces and collisions. The significance of both mechanisms could be assessed by defining taxonomic classes of a statistically significant sample of non-principal-axis rotators and compare them to spectra of known cometary nuclei.

The difficulty of observing the properties of tumbling asteroids is a clear factor against more extensive research on them. Extensive observations of slowly-rotating asteroids should be further extended and the methods used to solve the properties of the non-principal-axis rotators (Pravec et al. 2005) should be further developed to be able to solve the parameters of non-principal-axis rotators and their significance in the big picture of asteroid science.

References

Alvarez, L., Alvarez, W., Asaro, F. & Michel, H. (1980), 'Extraterrestrial cause for the Cretaceous-Tertiary extinction', *Science* **208**, 1095 – 1108.

Bottke, W. F., Durda, D. D., Nesvorný, D., Jedicke, R., Morbidelli, A., Vokrouhlický, D. & Levison, H. F. (2005), 'Linking the collisional history of the main asteroid belt to its dynamical excitation and depletion', *Icarus* **179**, 63 – 94.

Bowell, E., Oszkiewicz, D. A., Wasserman, L. H., Muinonen, K. & Trilling, D. E. (2013), 'Asteroid spin-axis longitudes from the Lowell Observatory database'. (submitted).

Carry, B., Kaasalainen, M., Merline, W. J., Müller, T. G., Jorda, L., Drummond, J. D., Berthier, J., O'Rourke, L., Ďurech, J., Küppers, M., Conrad, A., Tamblyn, P., Dumas, C., Sierks, H. & OSIRIS Team (2012), 'Shape modeling technique KOALA validated by ESA Rosetta at (21) Lutetia', *Planetary and Space Science* **66**, 200–212.

Cotto-Figueroa, D., Statler, T., Richardson, D. & Tanga, P. (2013), Radiation Recoil Effects on the Dynamical Evolution of Asteroids, *in* '44th Lunar and Planetary Science Conference'.

Ćuk, M. & Burns, J. A. (2005), 'Effects of thermal radiation on the dynamics of binary NEAs', *Icarus* **176**, 418 – 431.

Dobrovolskis, A. R. & Burns, J. A. (1984), 'Angular momentum drain – a mechanism for despinning asteroids', *Icarus* **57**, 464–476.

Ďurech, J. & Kaasalainen, M. (2003), 'Photometric signatures of highly nonconvex and binary asteroids', *Astronomy & Astrophysics* **404**, 709 – 714.

Ďurech, J., Kaasalainen, M., Warner, B. D., Fauerbach, M., Marks, S. A., Fauvaud, S., Fauvaud, M., Vugnon, J.-M., Pilcher, F., Bernasconi, L. & Behrend, R. (2009), 'Asteroid models from combined sparse and dense photometric data', *Astronomy & Astrophysics* **493**, 291 – 297.

Ďurech, J., Sidorin, V. & Kaasalainen, M. (2010), 'DAMIT: a database of asteroid models', *Astronomy & Astrophysics* **513**, A46.

Ďurech, J., Vokrouhlický, D., Kaasalainen, M., Higgins, D., Krugly, Y. N., Gaftonyuk, N. M., Shevchenko, V. G., Chiorny, V. G., Hamanowa, H., Hamanowa, H., Reddy, V. & Dyvig, R. R. (2008), 'Detection of the YORP effect in asteroid (1620) Geographos', *Astronomy & Astrophysics* **489**(2), L25 – L28.

Dymock, R. (2007), 'The H and G magnitude system for asteroids', *Journal of the British Astronomical Association* **117**(6), 342 – 343.

Foderà Serio, G., Manara, A. & Sikoli, P. (2002), *in* W. F. Bottke, A. Cellino, P. Paolicchi & R. P. Binzel, eds, 'Asteroids III', University of Arizona Press, chapter Guizeppe Piazzi and the discovey of Ceres, pp. 17–24.

Giorgini, J., Yeomans, D., Chamberlin, A., Chodas, P., Jacobson, R., Keesey, M., Lieske, J., Ostro, S., Standish, E. & Wimberly, R. (1996), 'JPL's On-Line Solar System Data Service', *Bulletin of the American Astronomical Society* **28**(3), 1158.

Gladman, B. J., Davis, D. R., Neese, C., Jedicke, R., Williams, G., Kavelaars, J. J., Petit, J.-M., Scholl, H., Holman, M., Warrington, B., Esquerdo, G. & Tricarico, P. (2009), 'On the asteroid belt's orbital and size distribution', *Icarus* pp. 104 – 118.

Granvik, M., Virtanen, J., Oszkiewicz, D. A. & Muinonen, K. (2009), 'OpenOrb: Open-source asteroid-orbit-computation software including statistical ranging', *Meteoritics and Planetary Science* **44**(12), 1853–1861.

Harris, A. W. (1994), 'Tumbling asteroids', *Icarus* **107**, 209–211.

Harris, A. W. (2002), 'On the slow rotation of asteroids', *Icarus* **156**, 184–190.

Harris, A. W. & Lagerros, J. S. V. (2002), *in* W. Bottke, A. Cellino, P. Paolicchi & R. P. Binzel, eds, 'Asteroids III', University of Arizona Press, chapter Asteroids in the Thermal Infrared, pp. 139–150.

Harris, A. W., Pravec, P. & Warner, B. D. (2012), 'Looking a gift horse in the mouth: Evaluation of wide-field asteroid photometric surveys ', *Icarus* **221**, 226–235.

Harris, A. W. & Young, J. W. (1983), 'Asteroid Rotation: IV. 1979 Observations', *Icarus* **54**, 59 – 109.

Harris, A., Young, J., Bowell, E., Martin, L., Millis, R., Poutanen, M., Scaltriti, F., Zappalà, V., Schober, H. J., Debehogne, H. & Zeigler, K. W. (1989), 'Photoelectric observations of asteroids 3, 24, 60, 261, and 863', *Icarus* **77**, 171–186.

Holsapple, K. A. (2007), 'Spin limits of Solar System bodies: From the small fast-rotators to 2003 EL61', *Icarus* **187**, 500 – 509.

Horner, J., Evans, N. W. & Bailey, M. E. (2004), 'Simulations of the population of Centaurs - I. The bulk statistics', *Monthly Notices of the Royal Astronomical Society* **354**(3), 798–810.

Husárik, M. (2012), 'Relative photometry of the possible main-belt comet (596) Scheila after an outburst', *Contributions of the Astronomical Observatory Skalnaté Pleso* **42**, 15–21.

IAU (2006), 'International Astronomical Union 2006 general assembly resolutions 5 and 6'.

Jewitt, D. (2009), Icy Bodies in the New Solar System, *in* J. Fernández, D. Lazzaro, D. Prialnik & R. Schulz, eds, 'Proceedings IAU Symposium No 263', Vol. 263 of *Proceedings of the International Astronomical Union*, Cambridge University Press, pp. 3 – 16.

Joye, W. A. & Mandel, E. (2003), New Features of SAOImage DS9, *in* H. E. Payne, R. I. Jedrzejewski & R. N. Hook, eds, 'Astronomical Data Analysis Software and Systems XII', Vol. 295 of *Astronomical Society of the Pacific Conference Series*, p. 489.

Kaasalainen, M. (2001), 'Interpretation of lightcurves of precessing asteroids', *Astronomy & Astrophysics* **376**, 302 – 309.

Kaasalainen, M., Mottola, S. & Fulchignoni, M. (2002), *in* W. Bottke, A. Cellino, P. Paolicchi & R. P. Binzel, eds, 'Asteroids III', University of Arizona Press, chapter Asteroids Models from disk-integrated Data, pp. 139–150.

Kaasalainen, M. & Torppa, J. (2001), 'Optimization Methods for Asteroid Lightcurve Inversion: I. Shape Determination', *Icarus* **153**, 24 – 36.

Kaasalainen, M., Torppa, J. & Muinonen, K. (2001), 'Optimization Methods for Asteroid Lightcurve Inversion: II. The Complete Inverse Problem', *Icarus* **153**, 37 – 51.

Kaasalainen, M., Ďurech, J., Warner, B. D., Krugly, Y. N. & Gaftonyuk, N. M. (2007), 'Acceleration of the rotation of asteroid 1862 Apollo by radiation torques', *Nature* **446**, 420 – 422.

Karttunen, H. (2009), *Vanhin tiede – tähtitiedettä kivikaudesta kuulentoihin*, Ursa.

Koskinen, H. E. & Vainio, R. (2010), *Klassinen mekaniikka*, Limes.

Kryszczyńska, A., La Spina, A., Paolicchi, P., Harris, A. W., Breiter, S. & Pravec, P. (2007), 'New findings on asteroid spin-vector distributions', *Icarus* **192**, 223 – 237.

Landau, L. D. & Lifshitz, E. M. (1965), *Mehanika*, Nauka.

Lowry, S. C., Fitzsimmons, A., Pravec, P., Vokrouhlický, D., Boehnhardt, H., Taylor, P. A., Margot, J.-L., Galád, A., Irwin, M., Irwin, J. & Kušnirák, P. (2007), 'Direct detection of the asteroidal YORP effect', *Science* **316**, 272 – 274.

Lucas, G. A. (2004), 'Modern Asteroid Occultation Observing Methods', *Society for Astronomical Sciences Annual Symposium* **23**, 85 – 100.

Magnusson, P., Lagerkvist, C.-I., Dahlgren, M., Erikson, A., Barucci, M. A., Belskaya, I. & Capria, M. T. (1994), The Uppsala Asteroid Data Base, *in* A. Milani, M. di Martino & A. Cellino, eds, 'Asteroids, Comets, Meteors 1993', Vol. 160 of *IAU Symposium*, pp. 471 – 476.

Mainzer, A., Grav, T., Bauer, J., Masiero, J., McMillan, R. S., Cutri, R. M., Walker, R., Wright, E., Eisenhardt, P., Tholen, D. J., Spahr, T., Jedicke, R.,

Denneau, L., DeBaun, E., Elsbury, D., Gautier, T., Gomillion, S., Hand, E., Mo, W., Watkins, J., Wilkins, A., Bryngelson, G. L., Del Pino Molina, A., Desai, S., Gómez Camus, M., Hidalgo, S. L., Konstantopoulos, I., Larsen, J. A., Maleszewski, C., Malkan, M. A., Mauduit, J.-C., Mullan, B. L., Olszewski, E. W., Pforr, J., Saro, A., Scotti, J. V. & Wasserman, L. H. (2011), 'NEOWISE Observations of Near-Earth Objects: Preliminary Results', *Astrophysical Journal* **743**, 156 – 173.

Marchis, F., Descamps, P., Hestroffer, D. & Berthier, J. (2005), 'Discovery of the triple asteroidal system 87 Sylvia', *Nature* **436**, 822 – 824.

Masiero, J., Jedicke, R., Ďurech, J., Gwyn, S., Denneau, L. & Larsen, J. (2009), 'The Thousand Asteroid Light Curve Survey', *Icarus* **204**, 145–171.

Merline, W. J., Close, L. M., Dumas, C., Chapman, C. R., Roddier, F., Ménard, F., Slater, D., Duvert, G., Shelton, C. & Morgan, T. (1999), 'Discovery of a moon orbiting the asteroid 45 Eugenia', *Nature* **401**, 565 – 568.

Michel, P., Benz, W., Tanga, P. & Richardson, D. C. (2001), 'Collisions and Gravitational Reaccumulation: Forming Asteroid Families and Satellites', *Science* **294**(5547), 1696 – 1700.

Michel, P., Morbidelli, A. & Bottke, W. F. (2005), 'Origin and dynamics of Near Earth Objects', *Comptes Rendus Physique* **6**, 291–301.

Milani, A., Knežević, Z., Novaković, B. & Cellino, A. (2010), 'Dynamics of the Hungaria asteroids', *Icarus* **207**, 769 – 794.

Muinonen, K., Belskaya, I. N., Cellino, A., Delbò, M., Levasseur-Regourd, A.-C., Penttilä, A. & Tedesco, E. F. (2010), 'A three-parameter magnitude phase function for asteroids', *Icarus* **209**, 542–555.

Nilsson, K., Takalo, L. & Piironen, J. (2006), *Havaitseva tähtitiede*, Ursa.

Noll, K. S., Weaver, H. L. & Feldman, P. D., eds (1996), *The collision of comet Shoemaker-Levy 9 and Jupiter*, Cambridge University Press.

Ostro, S. J., Hudson, R. S., Benner, L. A. M., Giorgini, J. D., Magri, C., Margot, J.-L. & Nolan, M. C. (2002), *in* W. F. Bottke, A. Cellino, P. Paolicchi & R. P. Binzel, eds, 'Asteroids III', University of Arizona Press, chapter Asteroid Radar Astronomy, pp. 151–168.

Oszkiewicz, D. A., Muinonen, K., Bowell, E., Trilling, A., Penttilä, A., Pieniluoma, T., Wasserman, L. H. & Enga, M. (2011), 'Online multi-parameter phase-curve fitting and application to a large corpus of asteroid photometric data', *Journal of Quantitative Spectroscopy and Radiative Transfer* **112**(11), 1919 – 1929.

Öpik, E. J. (1951), 'Collision probabilities with the planets and the distribution of interplanetary matter', *Proceedings of the Royal Irish Academy* **54A**, 165 – 199.

Pravec, P., Harris, A., Vokrouhlický, D., Warner, B. D., Kušnirák, P., Hornoch, K., Pray, D., Higgins, D., Oey, J., Galád, A., Gajdoš, Š., Kornoš, L., Világi, J., Husárik, M., Krugly, Y., Shevchenko, V., Chiorny, V., Gaftonyuk, N., Cooney Jr., W. R., Gross, J., Terrell, D., Stephens, R. D., Dyvig, R., Reddy, V., Ries, J. G., Colas, F., Lecacheux, J., Durkee, R., Masi, G., Koff, R. A. & Goncalves, R. (2008), 'Spin rate distribution of small asteroids', *Icarus* **197**, 497–504.

Pravec, P., Harris, A. W. & Michałowski, T. (2002), *in* W. F. Bottke, A. Cellino, P. Paolicchi & R. P. Binzel, eds, 'Asteroids III', University of Arizona Press, chapter Asteroid Rotations, pp. 113–122.

Pravec, P., Harris, A. W., Scheirich, P., Kušnirak, P., Šarounova, L., Hergenrother, C. W., Mottola, S., Hickse, M. D., Masi, G., Krugly, Y. N., Shevchenko, V. G., Nolan, N. C., Howell, E. S., Kaasalainen, M., Galád, A., Brown, P., DeGraff, D. R., Lambert, J. V., Cooney Jr., W. R. & Foglia, S. (2005), 'Tumbling asteroids', *Icarus* **173**, 108–131.

Pravec, P., Scheirich, P., Kušnirák, P., Šarounová, L., Mottola, S., Hahn, G., Brown, P., Esquerdo, G., Kaiser, N., Krzeminski, Z., Pray, D. P., Warner, B. D., Harris, A. W., Nolan, M. C., Howell, E. S., Benner, L. A. M., Margot, J.-L., Galád, A., Holliday, W., Hicks, M. D., Krugly, Y. N., Tholen, D., Whiteley, R., Marchis, F., Degraff, D. R., Grauer, A., Larson, S., Velichko, F. P., Cooney, W. R., Stephens, R., Zhu, J., Kirsch, K., Dyvig, R., Snyder, L., Reddy, V., Moore, S., Gajdoš, Š., Világi, J., Masi, G., Higgins, D., Funkhouser, G., Knight, B., Slivan, S., Behrend, R., Grenon, M., Burki, G., Roy, R., Demeautis, C., Matter, D., Waelchli, N., Revaz, Y., Klotz, A., Rieugné, M., Thierry, P., Cotrez, V., Brunetto, L. & Kober, G. (2006), 'Photometric survey of binary near-Earth asteroids', *Icarus* **181**, 63–93.

Rubincam, D. P. (2000), 'Radiative spin-up and spin-down of small asteroids', *Icarus* **148**(1), 2–11.

Salo, H. (1987), 'Numerical simulations of collisions between rotating particles', *Icarus* **70**, 37 – 51.

Samarasinha, N. H. & A'Hearn, M. F. (1991), 'Observational and Dynamical Constraints on the Rotation of Comet P/Halley', *The Astrophysical Journal Letters* **93**, 194 – 225.

Samarasinha, N. H., Mueller, B. E. A., A'Hearn, M. F., Farnham, T. L. & Gersch,

A. (2011), 'Rotation of comet 103P/Hartley 2 from structures in the coma', *The Astrophysical Journal Letters* **734**, L3.

Scheeres, D. J. & Sanchez, P. (2012), The Strength of Rubble Piles, *in* 'AAS/Division for Planetary Sciences Meeting Abstracts', Vol. 44 of *AAS/Division for Planetary Sciences Meeting Abstracts*, p. 105.03.

Shor, V. A., Zheleznov, N. B., Kochetova, O. M., Kuznetsov, V. B., Medvedev, Y. D., Netsvetaeva, G. A. & Chernetenko, Y. A., eds (2012), *Ephemerides of Minor Planets for 2013*, Institute of Applied Astronomy of Russian Academy of Sciences.

Smith, J. A., Tucker, D. L., Kent, S., Richmond, M. W., Fukugita, M., Ichikawa, T., Ichikawa, S., Jorgensen, A. M., Uomoto, A., Gunn, J. E., Hamabe, M., Watanabe, M., Tolea, A., Henden, A., Annis, J., Pier, J. R., McKay, T. A., Brinkmann, J., Chen, B., Holtzman, J., Shimasaku, K. & York, D. G. (2002), 'The *u'g'r'i'z'* Standard-Star System', *The Astronomical Journal* **123**(4), 2121 – 2144.

Spjuth, S. (2009), Disk-Resolved Photometry of Small Bodies, PhD thesis, Technischen Universität Carolo-Wilhelmina zu Braunschweig.

Tholen, D. J. & Barucci, M. A. (1989), *in* R. P. Binzel, T. Gehrels & M. S. Matthews, eds, 'Asteroids II', University of Arizona Press, chapter Asteroid taxonomy, pp. 298 – 315.

Tody, D. (1993), IRAF in the nineties, *in* R. Hanisch, R. Brissenden & J. Barnes, eds, 'Astronomical Data Analysis Software and Systems II', Vol. 52 of *A.S.P. Conference Series*, pp. 173+.

Vokrouhlický, D., Breiter, S., Nesvorný, D. & Bottke, W. F. (2007), 'Generalized

YORP evolution: Onset of tumbling and new asymptotic states', *Icarus* **191**, 636–650.

Vokrouhlický, D., Brož, M., Bottke, W. F., Nesvorný, D. & Morbidelli, A. (2006), 'Yarkovsky/YORP chronology of asteroid families', *Icarus* **182**, 118 – 142.

Vokrouhlický, D. & Farinella, P. (2000), 'Efficient delivery of meteorites to the Earth from a wide range of asteroid parent bodies', *Nature* **407**, 606–608.

Vokrouhlický, D. & Čapek, D. (2002), 'YORP-Induced Long-Term Evolution of the Spin State of Small Asteroids and Meteoroids: Rubincam's Approximation ', *Icarus* **159**, 449–467.

Warner, B. D., Harris, A. W. & Pravec, P. (2009a), 'The asteroid lightcurve database', *Icarus* **202**, 134 – 146.

Warner, B. D., Harris, A. W., Vokrouhlický, D., Nesvorný, D. & Bottke, W. F. (2009b), 'Analysis of the Hungaria asteroid population', *Icarus* **204**, 172 – 182.

Wilkman, O. & Muinonen, K. (2013), 'Asteroid lightcurve phase shift from rough-surface shadowing', *Meteoritics & Planetary Science* . (submitted).

Wirgin, A. (2004), 'The inverse crime', *arXiv* . math-ph/0401050.